

**21 cm angular-power spectrum from the dark ages**Antony Lewis<sup>1,\*</sup> and Anthony Challinor<sup>1,2</sup><sup>1</sup>*Institute of Astronomy, Madingley Road, Cambridge, CB3 0HA, United Kingdom*<sup>2</sup>*DAMTP, Centre for Mathematical Sciences, Wilberforce Road, Cambridge CB3 0WA, United Kingdom*  
(Received 26 February 2007; revised manuscript received 19 July 2007; published 17 October 2007)

At redshifts  $z \gtrsim 30$  neutral hydrogen gas absorbs cosmic microwave background radiation at the 21 cm spin-flip frequency. In principle this is observable and a high-precision probe of cosmology. We calculate the linear-theory angular-power spectrum of this signal and cross correlation between redshifts on scales much larger than the linewidth. In addition to the well-known redshift distortion and density perturbation sources, a full linear analysis gives additional contributions to the power spectrum. On small scales there is a percent-level linear effect due to perturbations in the 21 cm optical depth, and perturbed recombination modifies the gas temperature perturbation evolution (and hence spin temperature and 21 cm power spectrum). On large scales there are several post-Newtonian and velocity effects; although negligible on small scales, these additional terms can be significant at  $l \lesssim 100$  and can be nonzero even when there is no background signal. We also discuss the linear effect of reionization rescattering, which damps the entire spectrum and gives a very small polarization signal on large scales. On small scales we also model the significant nonlinear effects of evolution and gravitational lensing. We include full results for numerical calculation and also various approximate analytic results for the power spectrum and evolution of small-scale perturbations.

DOI: [10.1103/PhysRevD.76.083005](https://doi.org/10.1103/PhysRevD.76.083005)

PACS numbers: 98.70.Vc

**I. INTRODUCTION**

The cosmic microwave background (CMB) anisotropies have proved to be a valuable source of information about the initial conditions and evolution of the universe. Most current observations measure the CMB temperature and polarization assuming an exactly blackbody spectrum. However, by looking at the anisotropies as a function of frequency vastly more information can be obtained. In addition to the signal from secondary scattering in clusters, in principle there is also line absorption from sources along the line of sight. One of the most interesting of these is line absorption due to the 21 cm spin-flip transition in neutral hydrogen, giving a low frequency probe of the gas distribution at redshifts  $300 \gtrsim z \gtrsim 30$  [1–3]. This is sensitive to perturbations on all scales down to the Baryon Jeans' scale, which is orders of magnitude smaller than the photon-damping scale that limits what can be learned directly from the CMB temperature. The 21 cm absorption signal therefore potentially contains a huge amount of information about small-scale cosmological perturbations. Since the absorption signal from redshift  $z$  is observed at wavelength  $\lambda = (1+z)21.106$  cm [ $(1+z)\nu = 1420.4$  MHz], the signal can also be studied as a function of observed frequency to give tomographic information about the perturbations [2,4]. Unfortunately, observations at many-meter wavelengths are very challenging (see e.g. Refs. [3,5]), but make a useful target for next-but-one generation experiments.

The origin of the dark-age absorption signal is as follows. After recombination there is still a small fraction of

free electrons. Compton scattering transfers energy between CMB photons and the electrons (and hence the gas), and hence keeps the gas temperature close to the CMB temperature until a redshift of  $z \sim 300$ . At lower redshifts, the coupling becomes ineffective and the gas starts to cool adiabatically. Atomic collisions in the gas drive the atomic energy levels of the gas towards equilibrium with the gas temperature. The spin temperature defines the relative abundance of triplet and singlet hydrogen states, and is driven by collisions towards the gas temperature. Since the gas cools faster than the CMB, the spin temperature is below the CMB temperature, and 21 cm CMB photons will have net absorption by the gas. At redshifts  $z \lesssim 300$  an absorption signal may therefore be observable. At redshifts  $z \lesssim 30$  atomic collisions become very rare, and the spin temperature is driven back towards the CMB temperature by interaction with the numerous CMB photons. The absorption signal from the dark ages is therefore limited to  $30 \lesssim z \lesssim 300$ . At lower redshifts sources of Lyman- $\alpha$  photons and nonlinear effects become important, and again the spin temperature can depart from the CMB temperature, giving a signal in absorption or emission.

In this paper we focus on the absorption signal from  $z \gtrsim 30$  where the physics is well understood and much cleaner than the large uncertainties currently surrounding modeling at lower redshifts. We calculate the linear-theory angular-power spectrum of the 21 cm absorption as a function of redshift, including superhorizon scales where post-Newtonian effects may be important. We focus on the angular-power spectrum  $C_l(z, z')$  as this is what is directly observable. Many aspects of the physics may be much clearer with a reconstruction of the 3D power spectrum

\*URL: <http://cosmologist.info>

[6], but converting the observations into such a spectrum is in general nontrivial especially on large scales, and also dependent on assumptions about the cosmology. Since the perturbations should be nearly linear at high redshifts, the statistics should be close to Gaussian, and the angular-power spectra should encapsulate most of the statistical information in the observation. Our work extends that of Refs. [2,3,7–10] by including linear terms due to gravitational redshifting, all velocity effects, ionization fraction perturbations, self-absorption, and reionization rescattering. Corrections due to these extra terms are generally quite small, though percent-level effects will be very important if high-redshift 21 cm is ever going to fulfill its potential for constraining cosmology. We also estimate the effect of nonlinear evolution, which can be important on small scales even at high redshift, and calculate the effect due to gravitational lensing. Although we do not directly consider  $z \lesssim 30$  here, many of our results could easily be adapted to lower redshifts given a model of the Lyman- $\alpha$  sources and nonlinear clustering.

The CMB temperature anisotropy, sourced at  $z \sim 10^3$ , sees superhorizon perturbations at  $l \lesssim 100$ . For a 21 cm signal at  $z \sim 50$  the horizon scale is about 10 times larger, corresponding to an angular scale  $l \lesssim 10$ . One might therefore expect post-Newtonian effects to dominate at  $l < 10$ . However the small-scale 21 cm anisotropy is sourced by hydrogen density (and spin temperature and redshift distortion) fluctuations, which grow rapidly towards smaller scales. The large-scale signal is therefore dominated by fluctuations coming from much smaller scales. Since these smaller scales are uncorrelated on large scales, this gives an approximately white-noise 21 cm power spectrum on large angular scales. This white-noise signal dominates that from superhorizon scales, so the post-Newtonian corrections are generally below cosmic variance. In addition there are velocity effects, the most important of which is the dipole in the radiation field seen by each hydrogen atom due to its motion with respect to the CMB. This can give non-negligible quantitative corrections to the angular-power spectrum at  $l \lesssim 100$ .

On small scales Thomson scattering of 21 cm by the background reionization damps the entire spectrum and also induces a very small polarization signal. There are also additional 21 cm perturbation sources due to perturbations in the 21 cm optical depth; for example, an overdensity will have a slightly higher optical depth than the background, leading to a few-percent suppression in the absorption signal. Additional effects arise indirectly; in particular, inclusion of ionization fraction perturbations is important for the evolution of gas temperature fluctuations, and can modify the spectrum at all angular scales by a couple of percent.

The approach we adopt is to evolve the Boltzmann equation for the photon distribution function sourced by absorption of 21 cm radiation by neutral hydrogen. We

restrict our attention to a spatially flat close-to-Friedmann-Robertson-Walker cold-dark-matter (CDM) universe. Our results apply equally well with adiabatic or isocurvature scalar-mode initial conditions, though we only calculate the adiabatic mode spectra explicitly. We note in passing that 21 cm observations are potentially an excellent way to probe isocurvature modes, especially the compensated CDM-baryon mode that cannot be constrained from the CMB temperature [10,11]. We do not consider the tensor contribution to the intensity power spectrum as the effect is expected to be well below cosmic variance, though we do calculate the tiny tensor-induced polarization signal. We assume no significant particle decay or annihilations, and assume no variation of constants or non-Gaussianity, though these can be well constrained from their effect on the 21 cm signal if included [12–17].

We start by deriving the Boltzmann equation for the distribution function in linearized general relativity. The main linear-theory result relating the observable anisotropy on the sky to sources on the absorption surface is given in Eq. (18). On small scales the majority of the terms are negligible, and we give a result accurate on small scales in Eq. (22). This contains the usual density and spin-temperature fluctuation and redshift-distortion sources, but with additional few-percent terms due to the nonzero 21 cm optical depth that are often neglected. In Sec. III we then derive results for the angular-power spectrum in terms of linear-theory transfer functions. To actually calculate the power spectrum we need to calculate the sources, so in Sec. IV we give results for calculating the background and perturbed densities and temperatures. In Sec. V we describe the qualitative shape of the power spectrum, and give approximate semianalytic results for the large- and small-scale power spectrum. We then quantify the importance of the various effects in Sec. VI where we calculate the 21 cm intensity power spectrum numerically. The very small large-scale polarization signal is calculated in Sec. VII. Since the 21 cm power spectrum probes small scales, nonlinear evolution can in fact be important at the many-percent level even at redshift  $z \sim 50$ . We give an approximate estimate of the effect in Sec. VIII, and also give an accurate result for the lensed power spectrum in Sec. IX. A full nonlinear analysis is beyond the scope of this paper, but we briefly discuss other sources of nonlinear power in Sec. X. We finally conclude in Sec. XI. In a series of appendices, we give approximate results for the evolution of small-scale baryon perturbations, general-gauge results for numerical calculation, equations for the evolution of the ionization fraction perturbations, useful results for integrating spherical Bessel functions, and third-order perturbation theory results for the nonlinear CDM density and velocity power spectra.

The Boltzmann approach to calculating the line emission angular-power spectrum that we consider here is related to the angular-power spectrum of source number counts; we discuss this in a companion paper [18].

## II. BOLTZMANN EQUATION

At high redshift, perturbations should be close to linear, and we assume there are no sources of Lyman- $\alpha$  photons. During the dark ages the atomic collision time is comparable to the CMB photon interaction time, and for accurate results the full distribution of spin and velocity states must be accounted for [19]. To simplify our analysis we neglect this complication, focussing on new effects that arise from a full linear perturbation analysis when the spin temperature is independent of atomic velocity. The spin temperature during the dark ages is then governed by 21 cm interaction with CMB photons and atomic collisions. Since the collision rates are not known very accurately, and the ionization fraction after recombination is somewhat uncertain, the precision of our calculation is currently limited anyway. We also assume the background CMB temperature is exactly blackbody, neglecting any effects due to non-21 cm distortions, and assume that atomic angular momenta are isotropically distributed.

We employ linearized standard general relativity, working in the conformal Newtonian gauge with metric

$$ds^2 = a^2(\eta)[(1 + 2\psi)d\eta^2 - (1 - 2\phi)\delta_{ij}dx^i dx^j]. \quad (1)$$

Except when quoting a few results relevant for calculation of numerical answers, we use natural units with  $c = 1$ . We take a velocity field  $u^a$  to be along  $\partial_\eta$  so that  $u^\mu = a^{-1}(1 - \psi)\delta_0^\mu$  and  $u_\mu = a(1 + \psi)\delta_{\mu 0}$ . This velocity field is the zeroth element of an orthonormal tetrad which we take to be  $(X_0)^a = u^a$  and  $X_i \equiv a^{-1}(1 + \phi)\partial_i$ . Decomposing a photon wave vector  $k^a = dx^a/d\lambda$  into a direction  $e^a$  and frequency  $k \cdot u \equiv \epsilon/a$ , we have

$$\frac{d\mathbf{x}}{d\eta} = (1 + \phi + \psi)\mathbf{e}, \quad \frac{d\eta}{d\lambda} = a^{-2}\epsilon(1 - \psi), \quad (2)$$

where the three-vector  $\mathbf{e}$  comprises the spatial components of the propagation direction on the spatial triad  $X_i$ .

The number density of neutral hydrogen atoms is  $n_{HI} = n_0 + n_1$ , where the density in the ground state (degeneracy 1) is  $n_0$ , and the density in the upper triplet state (degeneracy 3) is  $n_1$ . We assume the spin temperature  $T_s$  is dependent only on time and position, defined by  $n_1/n_0 = 3e^{-T_s/T_s}$  where  $T_\star \equiv h_p \nu_{21}/k_B \approx 0.068$  K and  $\nu_{21}$  is the constant 21 cm frequency. In the rest frame of the gas the net number of 21 cm photons emitted per unit volume in proper time  $d\tau_g$  within energy  $dE$  within solid angle  $d\Omega$  is

$$dn_{21} = \frac{1}{4\pi}[(n_1 - 3n_0)\mathcal{N}_\nu + n_1] \times A_{10}\Phi(E - E_{21})d\tau_g dE d\Omega, \quad (3)$$

where  $E_{21}$  corresponds to the 21 cm frequency and  $\mathcal{N}_\nu$  is the photon phase space density controlling stimulated emission. The line profile  $\Phi(E - E_{21})$  is defined so that

$\int dE\Phi(E - E_{21}) = 1$ . The spontaneous emission rate  $A_{10} = 2\pi\alpha\nu_{21}^3 h_p^2 / (3c^4 m_e^2) \approx 2.869 \times 10^{-15} \text{ s}^{-1}$  [20], corresponding to a spontaneous decay time of  $\sim 10^7$  years and CMB photon interaction time  $\sim T_\star / (T_\gamma A_{10})$  (about  $10^4$  years at  $z = 30$ ). The form of the equation follows from considering detailed balance in equilibrium, in which there is no net production of photons at any temperature.

We shall only make an accurate calculation on scales larger than the linewidth. In this approximation we model the source emission as monochromatic, so that  $\Phi(E - E_{21}) = \delta(E - E_{21})$ . The thermal linewidth corresponds to scales with wave number of a few hundred  $\text{Mpc}^{-1}$  [4,19]. This unavoidability suppresses observed power on very small scales regardless of the observational bandwidth. On these scales power is also suppressed due to significant baryon pressure at earlier times, as discussed below. Observational bandwidth can be accounted for simply by integrating our final result over a frequency window function.

We model the radiation field as a CMB blackbody  $\mathcal{N}_p = (\exp(h_p \nu / k_B T_\gamma) - 1)^{-1}$  plus a term due to 21 cm emission  $\mathcal{N}_f$ . At the temperatures of interest where  $T_\star \ll T_\gamma$ , a good approximation is  $\mathcal{N}_p(\nu = \nu_{21}) = T_\gamma / T_\star$  so that  $\mathcal{N}_\nu = T_\gamma / T_\star + \mathcal{N}_f(\nu = \nu_{21})$ . Usually the photon temperature  $T_\gamma$  is taken to be isotropic, but here we are interested in corrections and so allow for its angular variation (e.g. due to the dipole in the rest frame of the atom). The gas-frame temperature is given by

$$T_\gamma^{(g)}(\mathbf{e}, \mathbf{x}, \eta) = \bar{T}_\gamma(\eta)[1 + \Theta(\mathbf{e}, \mathbf{x}, \eta) - \mathbf{e} \cdot \mathbf{v}(\mathbf{x}, \eta)], \quad (4)$$

where  $\Theta$  is the temperature perturbation and  $\mathbf{v}$  the gas (baryon) velocity relative to  $u^a$  on the  $X_i$  triad. Anisotropy in the radiation field may result in an anisotropic distribution of the atomic triplet states, which would significantly complicate our analysis. This will not be an issue if atomic collisions isotropize the distribution rapidly compared to the photon interaction time. However, during the dark ages the collision and photon interaction times are actually similar, so this may not be a safe assumption. Nonetheless, because the interaction is parity invariant, odd multipoles of the radiation field will not affect the triplet distribution; in particular, the dominant dipole term leaves an isotropic distribution unchanged. Higher-order CMB anisotropies will drive an anisotropy in the triplet distribution, however their relative amplitude is  $\sim 10^{-4}$  so their contribution is very small. Also the scattering time for a photon from the anisotropic part of the distribution will be longer than the collision time, so the distribution should in any case be randomized effectively. Similar comments apply to the effect of polarized radiation, so our approximation of an isotropic triplet distribution should be accurate.

If the gas 4-velocity is  $u_g^a$  the rest-frame energy is given by  $E^{(g)} = k_a u_g^a = \epsilon(1 - \mathbf{e} \cdot \mathbf{v})/a$ , and an interval  $d\lambda$  along

the photon path corresponds to a proper time  $d\tau_g = u_g^a dx_a = k_a u_g^a d\lambda$ . The Boltzmann equation for the evolution of the distribution function  $f$  (number density of photons  $f d\Omega E^2 dE/c^3 = 2\mathcal{N}_f d\Omega \nu^2 d\nu/c^3$ ) due to 21 cm interaction is then

$$\begin{aligned} \frac{df}{d\lambda} \Big|_H &= \frac{c^3 E_{21}}{4\pi E_{21}^2} \frac{3n_{HI} A_{10}}{3 + e^{T_*/T_s}} \left[ (1 - e^{T_*/T_s}) \left( \frac{T_\gamma^{(g)}}{T_\star} + \frac{h_p^3}{2} f \right) + 1 \right] \delta(k_a u_g^a - E_{21}) \\ &\approx \frac{3c^3 \bar{n}_{HI} A_{10}}{16\pi E_{21}} \left[ 1 + \Delta_{HI} - \frac{\bar{T}_\gamma (1 + \Theta - \mathbf{e} \cdot \mathbf{v} - \Delta_{T_s} + \Delta_{HI})}{\bar{T}_s} - \frac{h_p^3}{2} \frac{T_\star}{\bar{T}_s} \{ (\Delta_{HI} - \Delta_{T_s}) \bar{f} + f \} \right] \\ &\quad \times \delta(\epsilon(1 - \mathbf{e} \cdot \mathbf{v})/a - E_{21}), \end{aligned} \quad (5)$$

where  $n_{HI}$  is the number density of neutral hydrogen and we used the good approximation  $T_\star \ll T_s$ . We defined fractional perturbations in a quantity  $X$  as  $\Delta_X \equiv (\delta X)/\bar{X}$  and denoted background quantities by an overbar. Since the baryon pressure is very low, and the ionization fraction in the dark ages is small, we may take  $\Delta_{HI} = \Delta_H = \Delta_b$ , though the baryon perturbation  $\Delta_b$  can differ significantly from the CDM perturbation  $\Delta_c$ .

Although we do not model 21 cm emission from reionization in detail here, we do include rescattering of emission from higher redshift by the background electron density as this affects the power spectrum from the dark ages. For the moment we neglect polarization and discuss this later. The Thomson scattering contribution to the Boltzmann equation is then

$$\begin{aligned} \frac{df}{d\lambda} \Big|_{\text{Thomson}} &= E^{(g)} n_e \sigma_T \left[ \frac{3}{16\pi} \int d\tilde{\Omega} \tilde{\mathbf{e}}' \tilde{f}(E^{(g)}, \tilde{\mathbf{e}}') [1 + (\tilde{\mathbf{e}} \cdot \tilde{\mathbf{e}}')^2] - f(E, \mathbf{e}) \right] \\ &\approx E^{(g)} n_e \sigma_T \left[ \frac{3}{16\pi} \int d\Omega \mathbf{e}' f(E, \mathbf{e}') [1 + (\mathbf{e} \cdot \mathbf{e}')^2] - \mathbf{e} \cdot \mathbf{v} \epsilon \partial_\epsilon \bar{f} - f(E, \mathbf{e}) \right] \\ &\approx \frac{\epsilon \bar{n}_e \sigma_T}{a} \left[ F - \epsilon \partial_\epsilon \bar{f} \mathbf{e} \cdot \mathbf{v} + \frac{f_2}{10} - f \right], \end{aligned} \quad (6)$$

where  $F$  and  $f_2$  are the monopole and quadrupole parts of  $f$ . In the first line here, the tildes denote quantities in the gas frame evaluated on the Lorentz-boosted tetrad  $\tilde{X}_\mu$ .

The background equation does not depend on the Thomson scattering term. Defining

$$\bar{\rho}_s \equiv \frac{3c^3 \bar{n}_{HI} A_{10}}{16\pi E_{21}^2} \left( \frac{\bar{T}_s - \bar{T}_\gamma}{\bar{T}_s} \right), \quad (7)$$

the background equation becomes

$$\frac{\partial \bar{f}}{\partial \eta} = a \bar{\rho}_s \delta(\epsilon/a - E_{21}) - \dot{\tau} \bar{f}, \quad (8)$$

where the background optical depth to 21 cm is defined by

$$\begin{aligned} \bar{\tau}(\eta, \epsilon) &\equiv \int_0^\eta d\eta' \frac{3ac^3 \bar{n}_{HI} A_{10}}{16\pi E_{21}^2} \frac{h_p^3 T_\star}{2\bar{T}_s} \delta(\epsilon/a - E_{21}) \\ &= \left[ \frac{3\lambda_{21}^2 h_p c A_{10} \bar{n}_{HI}}{32\pi k_B \bar{T}_s H} \right]_\epsilon \theta(\eta - \eta_\epsilon) \equiv \tau_\epsilon \theta(\eta - \eta_\epsilon). \end{aligned} \quad (9)$$

Here  $\epsilon = a(\eta_\epsilon) E_{21}$ ,  $\theta(x)$  is the Heaviside function, and  $A$  denotes the observation point; a subscript  $\epsilon$  denotes the quantity is evaluated at time  $\eta_\epsilon$  [and additionally position  $\mathbf{x}_A + \hat{\mathbf{n}}(\eta_A - \eta_\epsilon)$  for perturbed quantities along a line of sight  $\hat{\mathbf{n}}$ ]. The optical depth  $\tau_\epsilon$  is quite small, typically 1%–4% over the epoch of most interest (see Fig. 2 below). The time derivative is given by

$$\dot{\tau} \equiv a \bar{\rho}_s \delta(\epsilon/a - E_{21}) = \tau_\epsilon \delta(\eta - \eta_\epsilon), \quad (10)$$

which defines the optical depth source  $\bar{\tau}_s(\eta)$  in analogy with  $\bar{\rho}_s$ .

The background solution is then given by the integral of Eq. (8),

$$\bar{f}(\eta, \epsilon) = \frac{1 - e^{-\bar{\tau}}}{\tau_\epsilon} \left[ \frac{a \bar{\rho}_s}{E_{21} \mathcal{H}} \right]_\epsilon \equiv \bar{f}(\epsilon) \frac{1 - e^{-\bar{\tau}}}{1 - e^{-\tau_\epsilon}}, \quad (11)$$

where  $\mathcal{H}$  is the conformal Hubble parameter and  $\bar{f}(\epsilon)$  is the value of  $\bar{f}(\eta, \epsilon)$  at  $\eta > \eta_\epsilon$ . To first order in  $\tau_\epsilon$  one can use  $\bar{f}(\eta, \epsilon) = \bar{f}(\epsilon) \theta(\eta - \eta_\epsilon)$ , however the full form given above must be used to get results correct to higher order in  $\tau_\epsilon$ . Predictions for the 21 cm power spectrum are often quoted in terms of the brightness temperature today, given by  $T_b = E_{\text{obs}} h_p^3 f / 2k_B$ . The isotropic brightness today due to background emission is therefore

$$\bar{T}_b(\eta_A, \epsilon) = (1 - e^{-\tau_\epsilon}) \frac{\bar{T}_s - \bar{T}_\gamma}{1 + z} \Big|_\epsilon. \quad (12)$$

During the dark ages, the spin temperature is below the CMB temperature, so  $\bar{T}_b$  is negative corresponding to net absorption.

To calculate the perturbation to the distribution function we define the monopole source

$$\Delta_s \equiv \Delta_{HI} + \frac{\bar{T}_\gamma}{\bar{T}_s - \bar{T}_\gamma} (\Delta_{T_s} - \Delta_{T_\gamma}). \quad (13)$$



The total perturbed Boltzmann equation then becomes

$$\begin{aligned} \frac{df}{d\lambda} = & E_{21} \left[ \bar{\rho}_s \left[ 1 + \Delta_s - \frac{\bar{T}_\gamma}{\bar{T}_s - \bar{T}_\gamma} \{ \mathbf{e} \cdot (\mathbf{v}_\gamma - \mathbf{v}) + \Theta_+ \} \right] \right. \\ & \left. - \bar{\tau}_s [ \{ (\Delta_{HI} - \Delta_{T_s}) \bar{f} + f \} ] \right] \delta(\epsilon(1 - \mathbf{e} \cdot \mathbf{v})/a - E_{21}) \\ & + \frac{\epsilon \bar{n}_e \sigma_T}{a} \left[ F - \epsilon \partial_\epsilon \bar{f} \mathbf{e} \cdot \mathbf{v} + \frac{f_2}{10} - f \right]. \end{aligned} \quad (14)$$

Here  $\Theta_+$  denotes the gauge-invariant temperature anisotropy sources with  $l \geq 2$ , and  $\mathbf{v}_\gamma$  is the velocity (i.e. dipole) of the photon distribution.

To solve the perturbed Boltzmann equation, we use the time component of the geodesic equation, which reduces to an equation for the evolution of the comoving energy along the line of sight:

$$\frac{d\epsilon}{d\eta} = -\epsilon \frac{d\psi}{d\eta} + \epsilon(\dot{\phi} + \dot{\psi}), \quad (15)$$

where overdots denote conformal-time partial derivatives. We parametrize the distribution function in the Newtonian gauge as  $f(\eta, \mathbf{x}, \epsilon, \mathbf{e})$ , in which case the Boltzmann equation becomes

$$\begin{aligned} \frac{\partial f}{\partial \eta} + \mathbf{e} \cdot \nabla f + \epsilon \partial_\epsilon \bar{f} \left( \dot{\phi} + \dot{\psi} - \frac{d\psi}{d\eta} \right) = & a \bar{\rho}_s \left[ 1 + \Delta_s + \psi - \mathbf{e} \cdot \mathbf{v} - \frac{\bar{T}_\gamma}{\bar{T}_s - \bar{T}_\gamma} \{ \mathbf{e} \cdot (\mathbf{v}_\gamma - \mathbf{v}) + \Theta_+ \} \right] \delta(\epsilon/a - E_{21}) \\ & - (\Delta_{HI} - \Delta_{T_s} + \psi - \mathbf{e} \cdot \mathbf{v}) \dot{\bar{f}} - \dot{\bar{f}} - \mathbf{e} \cdot \mathbf{v} (\dot{\tau} \epsilon \partial_\epsilon \bar{f} + \epsilon \partial_\epsilon \dot{\bar{f}}) \\ & + \dot{\tau}_c \left[ \epsilon \partial_\epsilon \bar{f} \mathbf{e} \cdot \mathbf{v} - \frac{f_2}{10} + f - F \right], \end{aligned} \quad (16)$$

where  $\tau_c$  is the Thomson scattering optical depth. Noting that  $\epsilon \partial_\epsilon = \mathcal{H}_\epsilon^{-1} \partial_{\eta_\epsilon}$ , we have from Eq. (11)

$$\epsilon \partial_\epsilon \bar{f}(\eta, \epsilon) = \bar{f}_{,\text{ln}\epsilon}(\epsilon) \frac{1 - e^{-\bar{\tau}}}{1 - e^{-\tau_\epsilon}} - \frac{\bar{f}(\epsilon)}{\mathcal{H}_\epsilon} \frac{\dot{\bar{\tau}} e^{-\bar{\tau}}}{1 - e^{-\tau_\epsilon}}, \quad (17)$$

which defines an additional time-independent quantity  $\bar{f}_{,\text{ln}\epsilon}(\epsilon)$ . Substituting into the Boltzmann equation and integrating formally along the background line of sight gives the final result:

$$\begin{aligned} \delta f(\eta_A, \mathbf{x}_A, \epsilon, \hat{\mathbf{n}}) = & e^{-\tau_c} \bar{f}(\epsilon) \left[ \Delta_s + \psi + \hat{\mathbf{n}} \cdot \mathbf{v} + \frac{\bar{T}_\gamma}{\bar{T}_s - \bar{T}_\gamma} \{ \hat{\mathbf{n}} \cdot (\mathbf{v}_\gamma - \mathbf{v}) - \Theta_+ \} \right. \\ & + \frac{\tau_\epsilon e^{-\tau_\epsilon}}{\mathcal{H}_\epsilon (1 - e^{-\tau_\epsilon})} \left( -\frac{d\psi}{d\eta} + (\dot{\phi} + \dot{\psi}) + \hat{\mathbf{n}} \cdot \frac{d\mathbf{v}}{d\eta} \right) \Big|_\epsilon + e^{-\tau_c} \bar{f}_{,\text{ln}\epsilon}(\epsilon) (e^{\tau_c} \psi_A - \psi_\epsilon + \hat{\mathbf{n}} \cdot \mathbf{v}_\epsilon) \\ & - \bar{f}_{,\text{ln}\epsilon}(\epsilon) \int_{\eta_\epsilon}^{\eta_A} d\eta e^{-\tau_c} (\dot{\phi} + \dot{\psi}) + e^{-\tau_c} \bar{f}(\epsilon) \left( \frac{\tau_\epsilon e^{-\tau_\epsilon}}{1 - e^{-\tau_\epsilon}} - 1 \right) [\Delta_{HI} - \Delta_{T_s} + \psi + \hat{\mathbf{n}} \cdot \mathbf{v}]_\epsilon \\ & - \int_{\eta_\epsilon}^{\eta_A} d\eta \dot{\tau}_c e^{-\tau_c} \left( \delta f_0 + \bar{f}_{,\text{ln}\epsilon}(\epsilon) (\hat{\mathbf{n}} \cdot \mathbf{v} - \psi) + \frac{f_2}{10} \right), \end{aligned} \quad (18)$$

where  $\hat{\mathbf{n}} = -\mathbf{e}|_A$  and  $\epsilon < a_A E_{21}$  (i.e. observed energy strictly less than  $E_{21}$ ), and  $\delta f_0$  is the monopole perturbation. We have assumed that the CMB anisotropies can be well observed at higher frequencies, and the first-order perturbation from last scattering subtracted off the 21 cm map. The 21 cm brightness fluctuation calculated here is then that of the difference map without the blackbody contribution. We have also assumed there is no overlap between reionization and the 21 cm absorption.

The first term in Eq. (18) is the usual monopole source, with additional terms  $\psi + \hat{\mathbf{n}} \cdot \mathbf{v}$  reflecting the additional emission due to the difference between proper time in the gas frame and the interval  $d\eta$  along the line of sight. Then there is the effect from the CMB dipole seen in the gas frame,  $\mathbf{v}_\gamma - \mathbf{v}$ , plus higher multipole contributions to the temperature seen by the source,  $\Theta_+$ . The remaining terms on the first line of Eq. (18) describe the local effect of

gravitational and Doppler redshifting on the relation between an observed redshift interval  $\Delta z$  and the  $\Delta\eta$  along the line of sight. The main such redshift-distortion effect comes from the radial gradient contribution to  $\hat{\mathbf{n}} \cdot (d\mathbf{v}/d\eta)$ . The term multiplying  $\bar{f}_{,\text{ln}\epsilon}(\epsilon)$  is just  $\mathcal{H} \delta\eta$ , where  $\delta\eta$  is the perturbation to the conformal time for a fixed (gas-frame) redshift surface; it has the usual Doppler, Sachs-Wolfe, and integrated Sachs-Wolfe contributions familiar from CMB studies. The first term on the third line describes the perturbation to the 21 cm optical depth: for small  $\tau_\epsilon$  the term is proportional to  $\tau_\epsilon/2$ , corresponding to 21 cm photons on average seeing half of the perturbation along their line of sight.

To understand the way in which reionization enters Eq. (18), consider reionization approximated by a delta-function visibility function at time  $\eta_{\text{re}}$  with optical depth  $\tau_c$ . Dropping self-scattering terms (taking  $\tau_\epsilon \rightarrow 0$ ), we

then have

$$\begin{aligned} \delta f(\eta_A, \mathbf{x}_A, \boldsymbol{\epsilon}, \hat{\mathbf{n}}) &= e^{-\tau_c} \bar{f}(\boldsymbol{\epsilon}) \left[ \Delta_s + \psi + \hat{\mathbf{n}} \cdot \mathbf{v} + \frac{\bar{T}_\gamma}{\bar{T}_s - \bar{T}_\gamma} \{ \hat{\mathbf{n}} \cdot (\mathbf{v}_\gamma - \mathbf{v}) - \Theta_+ \} + \frac{1}{\mathcal{H}} \left( -\frac{d\psi}{d\eta} + (\dot{\phi} + \dot{\psi}) + \hat{\mathbf{n}} \cdot \frac{d\mathbf{v}}{d\eta} \right) \right]_\epsilon \\ &+ e^{-\tau_c} \bar{f}_{,\text{line}}(\boldsymbol{\epsilon}) \left( \psi_A - \psi_\epsilon + \hat{\mathbf{n}} \cdot \mathbf{v}_\epsilon - \int_{\eta_\epsilon}^{\eta_A} d\eta (\dot{\phi} + \dot{\psi}) \right) \\ &+ (1 - e^{-\tau_c}) \bar{f}_{,\text{line}}(\boldsymbol{\epsilon}) \left( \psi_A - \psi_{\text{re}} + \hat{\mathbf{n}} \cdot \mathbf{v}_{\text{re}} - \int_{\eta_{\text{re}}}^{\eta_A} d\eta (\dot{\phi} + \dot{\psi}) \right) + (1 - e^{-\tau_c}) \left( \delta f_0(\boldsymbol{\epsilon}) + \frac{1}{10} f_2(\boldsymbol{\epsilon}, \mathbf{e}) \right)_{\text{re}}. \end{aligned} \quad (19)$$

The first two sets of terms are the  $\delta f$  without reionization multiplied by the fraction,  $e^{-\tau_c}$ , of 21 cm photons that are not rescattered. The third set contains the effective  $\delta\eta$  for those photons that do rescatter (i.e. only the common part that is accrued after reionization) weighted by the fraction,  $1 - e^{-\tau_c}$ , that scatter. Finally, the fourth terms arise from in-scattering at reionization and represents an average of the source functions on the electrons' 21 cm surface. For perturbation modes with  $k(\eta_{\text{re}} - \eta_\epsilon) \gg 1$ , the dominant contribution to the 21 cm monopole at reionization is  $\delta f_0(\boldsymbol{\epsilon})|_{\text{re}} \approx \bar{f}_{,\text{line}}(\boldsymbol{\epsilon})\psi|_{\text{re}}$  since the source terms on the electrons' 21 cm surface average to zero. Using this in Eq. (19), we see that for such modes reionization damps the 21 cm anisotropies by  $e^{-\tau_c}$ . For modes with  $k(\eta_{\text{re}} - \eta_\epsilon) \ll 1$ , reionization has essentially no effect since scattering out of the line of sight is balanced by in-scattering. However, the contribution from such modes (which were necessarily outside the horizon at  $\eta_\epsilon$ ) to the 21 cm anisotropy at any multipole  $l$  is now small since there is considerably more power in modes with larger  $k$  (see Sec. V). The net effect is that reionization should suppress the 21 cm anisotropies by  $e^{-\tau_c}$  on all scales, unlike the CMB where there is no suppression at large  $l$ .

On small scales (well inside the horizon) most of the terms are completely negligible. Defining  $r_\tau \equiv \tau_\epsilon e^{-\tau_\epsilon} / (1 - e^{-\tau_\epsilon})$  Eq. (18) is approximated by

$$\begin{aligned} \delta f(\eta_A, \mathbf{x}_A, \boldsymbol{\epsilon}, \hat{\mathbf{n}}) &\approx e^{-\tau_c} \bar{f}(\boldsymbol{\epsilon}) \left[ \Delta_s - \frac{r_\tau}{\mathcal{H}_\epsilon} \hat{\mathbf{n}} \cdot \frac{\partial \mathbf{v}}{\partial \chi} + (r_\tau - 1) \right. \\ &\quad \left. \times (\Delta_{HI} - \Delta_{T_s}) \right]_\epsilon \end{aligned} \quad (20)$$

$$\approx e^{-\tau_c} \bar{f}(\boldsymbol{\epsilon}) \left[ \Delta_s - \frac{1}{\mathcal{H}} \hat{\mathbf{n}} \cdot \frac{\partial \mathbf{v}}{\partial \chi} \right]_\epsilon, \quad (21)$$

where  $\chi \equiv \eta_A - \eta$  is the conformal distance along the line of sight. The result in the first line should be very

accurate on small scales. In the second line, we made the approximation that  $\tau_\epsilon \sim 0$ ,  $r_\tau \sim 1$  to recover the standard approximation that is only accurate to  $\mathcal{O}(\tau_\epsilon)$  (percent level). Neglecting small photon perturbations, Eq. (20) can also be written as an expression for the brightness perturbation today

$$\begin{aligned} \delta T_b(\eta_A, \mathbf{x}_A, \boldsymbol{\epsilon}, \hat{\mathbf{n}}) &= \frac{e^{-\tau_c}}{1 + z_\epsilon} \left[ \tau_\epsilon e^{-\tau_\epsilon} (\bar{T}_s - \bar{T}_\gamma) \right. \\ &\quad \times \left( \Delta_{HI} - \Delta_{T_s} - \frac{1}{\mathcal{H}_\epsilon} \hat{\mathbf{n}} \cdot \frac{\partial \mathbf{v}}{\partial \chi} \right) \\ &\quad \left. + (1 - e^{-\tau_\epsilon}) \bar{T}_s \Delta_{T_s} \right]_\epsilon. \end{aligned} \quad (22)$$

To consider the impact of the additional terms on large scales we next derive an expression for the power spectrum for numerical calculation.

### III. ANGULAR-POWER SPECTRUM

For numerical work, one can expand into multipoles and harmonics. We use

$$\begin{aligned} \delta f(\boldsymbol{\eta}, \mathbf{x}, \boldsymbol{\epsilon}, \mathbf{e}) &= \sum_{l \geq 0} \int \frac{d^3 \mathbf{k}}{(2\pi)^{3/2}} (-i)^l (2l + 1) \\ &\quad \times F_l(\boldsymbol{\eta}, \boldsymbol{\epsilon}, \mathbf{k}) P_l(\hat{\mathbf{k}} \cdot \mathbf{e}) e^{i\mathbf{k} \cdot \mathbf{x}} \\ &= 4\pi \sum_{lm} \int \frac{d^3 \mathbf{k}}{(2\pi)^{3/2}} (-i)^l F_l(\boldsymbol{\eta}, \boldsymbol{\epsilon}, \mathbf{k}) \\ &\quad \times Y_{lm}^*(\hat{\mathbf{k}}) Y_{lm}(\mathbf{e}) e^{i\mathbf{k} \cdot \mathbf{x}}, \end{aligned} \quad (23)$$

$$\mathbf{v}_i(\boldsymbol{\eta}, \mathbf{x}) = \int \frac{d^3 \mathbf{k}}{(2\pi)^{3/2}} (-i) v_i(\boldsymbol{\eta}, \mathbf{k}) \hat{\mathbf{k}} e^{i\mathbf{k} \cdot \mathbf{x}}, \quad (24)$$

for the  $i$ th species, and similarly for the temperature multipoles, giving

$$\begin{aligned}
F_l(\eta_A, \boldsymbol{\epsilon}, \mathbf{k}) = & e^{-\tau_c} \left\{ \bar{f}(\boldsymbol{\epsilon}) \left[ \Delta_s + \psi + \frac{r_\tau \dot{\phi}}{\mathcal{H}} + (r_\tau - 1)(\Delta_{HI} - \Delta_{T_s} + \psi) \right]_\epsilon - \bar{f}_{,\ln\epsilon}(\boldsymbol{\epsilon}) \psi_\epsilon \right\} j_l(k\chi_\epsilon) \\
& - e^{-\tau_c} \left[ \frac{r_\tau \bar{f}(\boldsymbol{\epsilon})}{\mathcal{H}} (\dot{v} + \mathcal{H}v - k\psi) + \bar{f}_{,\ln\epsilon}(\boldsymbol{\epsilon}) v + \bar{f}(\boldsymbol{\epsilon}) \frac{\bar{T}_\gamma}{\bar{T}_s - \bar{T}_\gamma} (v_\gamma - v) \right]_\epsilon j'_l(k\chi_\epsilon) \\
& + r_\tau e^{-\tau_c} \bar{f}(\boldsymbol{\epsilon}) \frac{k v_\epsilon}{\mathcal{H}} j'_l(k\chi_\epsilon) - \int_{\eta_\epsilon}^{\eta_A} d\eta \tau_c e^{-\tau_c} \left[ (F_0 - \bar{f}_{,\ln\epsilon}(\boldsymbol{\epsilon}) \psi) j_l(k\chi) - \bar{f}_{,\ln\epsilon}(\boldsymbol{\epsilon}) v j'_l(k\chi) \right. \\
& + \left. \frac{F_2}{4} \{3j''_l(k\chi) + j_l(k\chi)\} \right] - \bar{f}_{,\ln\epsilon}(\boldsymbol{\epsilon}) \int_{\eta_\epsilon}^{\eta_A} d\eta e^{-\tau_c} (\dot{\phi} + \dot{\psi}) j_l(k\chi) \\
& - e^{-\tau_c} \bar{f}(\boldsymbol{\epsilon}) \frac{\bar{T}_\gamma}{\bar{T}_s - \bar{T}_\gamma} \sum_{l'=2}^{\infty} (2l' + 1) \Theta_{l'} i^{l'} P_{l'} \left( -\frac{i}{k} \frac{d}{d\chi_\epsilon} \right) j_l(k\chi_\epsilon) \quad (25)
\end{aligned}$$

for  $l \geq 1$ , where a prime denotes a derivative with respect to the argument. The  $\Theta_l$  are the angular moments of the Fourier expansion of the CMB temperature anisotropy and are defined analogously to  $F_l$ . The last term is small, of the order of the  $l \geq 2$  CMB temperature fluctuation. Note that  $\dot{v} + \mathcal{H}v - k\psi$  is zero in the absence of Thomson scattering or baryon pressure effects. Equation (25) can be integrated over a given frequency window function (determined by the observation) to determine the actual observed power. If desired one can integrate by parts so that the result depends only on  $j_l$  and derivatives of the window function and sources. We perform our numerical calculations this way in the synchronous gauge: the equations in a general gauge are given in Appendix B.

The angular-power spectrum is given by

$$C_l(z, z') = 4\pi \int d \ln k \mathcal{P}_\chi(k) F_l(k, z) F_l(k, z'), \quad (26)$$

where  $\mathcal{P}_\chi$  is the power spectrum of the primordial curvature perturbation  $\chi$  and  $F_l(k, z)$  is the distribution function multipole transfer function to redshift  $z = a_A E_{21}/\epsilon - 1$ ; i.e.  $F_l(k, z) = F_l(\eta_A, E_{21}/(1+z), \mathbf{k})$  for unit initial curvature perturbation.

To calculate the sources for the line-of-sight integral, we need to compute the perturbations in the spin and gas temperatures, and, for reionization, the evolution of the low multipoles of the distribution function. We consider these next.

#### IV. EVOLUTION

The evolution of the spin temperature is determined from the evolution equation for the states of a fixed number of atoms  $N_{HI} = N_0 + N_1$  in the gas rest frame. If we crudely assume that recombinations are to the singlet and triplet state in the ratio 1:3, we have

$$\begin{aligned}
\frac{\partial N_0}{\partial \tau} = & -N_0(C_{01} + 3A_{10} \mathcal{N}_{\nu 0}) + N_1(C_{10} + A_{10}(1 + \mathcal{N}_{\nu 0})) \\
& - \frac{\partial x_e}{\partial \tau} \frac{N_{HI} + N_e}{4}, \quad (27)
\end{aligned}$$

where  $\tau$  is the gas proper time,  $\mathcal{N}_{\nu 0}$  the monopole part of

$\mathcal{N}_\nu$  in the gas rest-frame integrated over the line profile (evaluated in Appendix C), and the ionization fraction is  $x_e \equiv n_e/n_H \equiv n_e/(n_{HI} + n_e)$  (we are neglecting molecular hydrogen and assume all helium is neutral). Here the collision term is  $C_{10} = \kappa_{10}^{HH} n_{HI} + \kappa_{10}^{eH} n_e + \kappa_{10}^{pH} n_p$  and  $C_{01} = 3C_{10} e^{-T_*/T_g}$ , where  $T_g$  is the gas temperature. The rates  $\kappa_{10}^i$  for hydrogen-hydrogen, hydrogen-electron, and hydrogen-proton collisional coupling are taken from Refs. [3,21] (fit using a cubic splines and 5th order polynomial in the logs), and not known to an accuracy of better than a few percent. As shown in Fig. 1, the hydrogen-hydrogen term dominates because of the small dark-age ionization fraction ( $x_e \sim 2 \times 10^{-4}$ ), and proton-hydrogen rates are suppressed relative to electron-hydrogen rates by a factor of  $\sim (m_e/m_p)^{1/2}$  due to the lower proton velocity, except at low redshifts where the proton cross section is significantly higher [21]. We include the small correction from electron-hydrogen collisions, but neglect the proton-hydrogen term.

At redshift  $z \sim 70$  the total collisional and photon interaction rates are about equal,  $C_{10} \sim T_\gamma A_{10}/T_*$ , with  $C_{10} \sim 10^{-11} \text{ s}^{-1}$  (corresponding to a collisional coupling time  $\sim 4000$  yr). At lower redshifts the gas becomes diffuse and collisions become less effective at coupling the spin temperature to the gas temperature. Defining  $\beta_s \equiv 1/T_s$  (etc.), the evolution of the spin temperature is determined by

$$\begin{aligned}
\frac{\partial \beta_s}{\partial \tau} + \frac{\beta_s}{1 - x_e} \frac{\partial x_e}{\partial \tau} = & 4[(\beta_g - \beta_s)C_{10} \\
& + \beta_\star(1 - \beta_s[T_\gamma + T_{b0}])A_{10}], \quad (28)
\end{aligned}$$

where  $T_\gamma + T_{b0} = T_* \mathcal{N}_{\nu 0}$  is the (perturbed) monopole brightness temperature. For scales large compared to the narrow line profile, we have

$$\begin{aligned}
T_\gamma + T_{b0} = & T_\gamma + \frac{1}{2} \hat{\tau}_\eta (T_s - T_\gamma) \\
= & \bar{T}_\gamma (1 + \Delta_{T_\gamma}) + \frac{\bar{T}_\eta}{2} (\bar{T}_s - \bar{T}_\gamma) \\
& \times \left[ 1 + \Delta_s + \psi + \frac{1}{\mathcal{H}} \left( \dot{\phi} - \frac{1}{3} \nabla \cdot \mathbf{v} \right) \right] \quad (29)
\end{aligned}$$

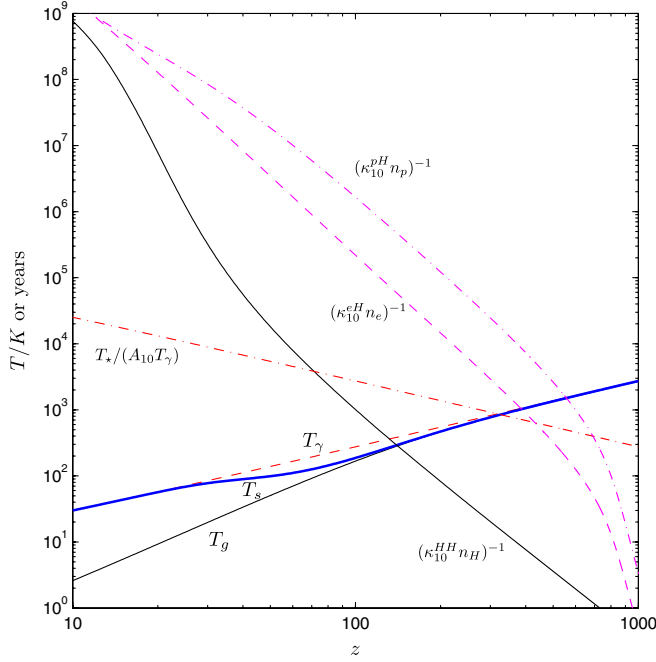


FIG. 1 (color online). Evolution of the interaction times for H-H, H-e, H-p, and H-photon spin-coupling processes, and how this influences the spin temperature  $T_s$  relative to the background CMB and gas temperatures. At high temperatures the H-H collision time is short and collisions couple  $T_s$  to the gas temperature  $T_g$ ; at lower redshifts the gas is diffuse and CMB photon interactions drive  $T_s$  to the CMB temperature  $T_\gamma$ . This figure assumes purely linear evolution and no Lyman- $\alpha$  coupling; in reality nonlinear effects are likely to change the result at  $z \lesssim 30$ .

to first order in the small optical depth  $\tau_\eta \equiv \tau_{\epsilon_\eta}$  (see Appendix C). The quantity

$$\hat{\tau}_\eta \equiv \frac{9\lambda_{21}^2 h_p c A_{10} n_{HI}}{32\pi k_B T_s \nabla_a u_g^a} \quad (30)$$

is the perturbed optical depth to 21 cm, where  $\nabla_a u_g^a$  is the volume expansion rate of the gas. Note that  $T_s \hat{\tau}_\eta$  is independent of the (perturbed) spin temperature. Since  $\tau_\eta$  is small, and the relevant nonperturbative equation in  $\tau_\eta$  cannot be easily solved, we make this first-order approximation below. In the epoch before reionization the spin temperature and ionization fraction only vary on Hubble time scales. The coupling time is short compared to the Hubble time, so the spin temperature is determined to very good accuracy by equilibrium, with the left-hand side of Eq. (28) being zero,

$$T_s \approx T_\gamma \left( \frac{C_{10} T_\star / T_\gamma + A_{10}}{C_{10} T_\star / T_g + A_{10}} \right) + \frac{1}{2} T_s \hat{\tau}_\eta A_{10} \left( \frac{1}{C_{10} T_\star / T_g + A_{10}} - \frac{1}{C_{10} T_\star / T_\gamma + A_{10}} \right). \quad (31)$$

The spin temperature varies between  $T_\gamma$  and  $T_g$  depending on whether the radiation or collision terms dominate; see Fig. 1. The second term in Eq. (31) due to the finite 21 cm optical depth is generally very small, giving a correction to the spin temperature of less than half a percent, and to  $T_\gamma - T_s$  of at most about 1%. The small effect on the brightness is shown in Fig. 2. This is smaller than the correction due to our assumption of a single velocity-independent spin temperature [19].

The perturbations to the spin temperature are determined by

$$\begin{aligned} \Delta T_s - \Delta T_\gamma = & (R_\gamma - R_g) \delta C_{10} + C_{10} (R_g \Delta T_g - R_\gamma \Delta T_\gamma) \\ & + \frac{1}{2} \tau_\eta A_{10} C_{10} \frac{\bar{T}_g - \bar{T}_\gamma}{T_\star} R_g R_\gamma \left[ \Delta_{HI} + \psi \right. \\ & + \frac{1}{\mathcal{H}} \left( \dot{\phi} - \frac{1}{3} \nabla \cdot \mathbf{v} \right) + \Delta C_{10} \\ & + 2\Delta T_\gamma (C_{10} R_\gamma - 1) - 2R_\gamma \delta C_{10} \\ & \left. + \frac{\bar{T}_\gamma}{\bar{T}_g - \bar{T}_\gamma} (\Delta T_g - \Delta T_\gamma) \right], \quad (32) \end{aligned}$$

where  $R_i^{-1} \equiv (C_{10} + A_{10} \bar{T}_i / T_\star)$  and

$$\begin{aligned} \delta C_{10} = & \Delta_H C_{10} + \left[ \frac{d \ln \kappa_{10}^{HH}}{d \ln T_g} (1 - \bar{x}_e) \kappa_{10}^{HH} \right. \\ & + \left. \frac{d \ln \kappa_{10}^{eH}}{d \ln T_g} \bar{x}_e \kappa_{10}^{eH} \right] \bar{n}_H \Delta T_g \\ & + (\kappa_{10}^{eH} - \kappa_{10}^{HH}) \bar{x}_e \bar{n}_H \Delta x_e. \end{aligned}$$

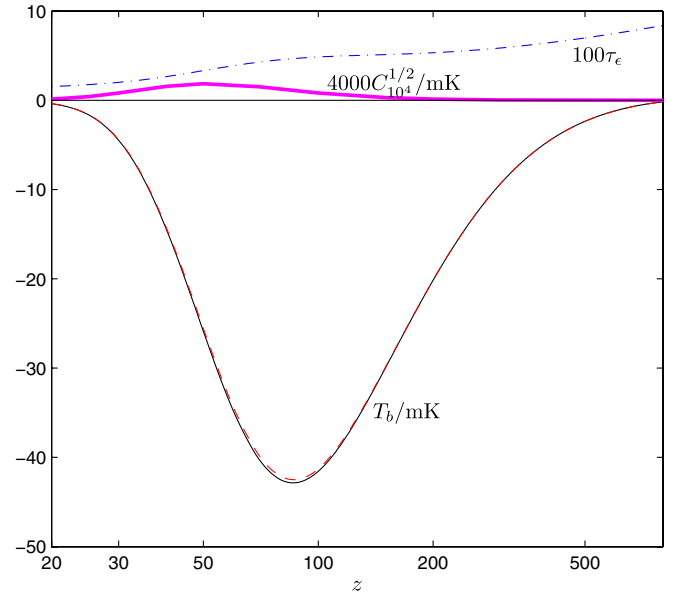


FIG. 2 (color online). The background 21 cm brightness  $T_b$ , optical depth  $\tau_\epsilon$ , and  $[l(l+1)C_l/2\pi]^{1/2}$  at  $l = 10^4$  as a function of source redshift. The dashed line shows the result for  $T_b$  neglecting the second term in Eq. (31) due to the effect of absorption on the ambient blackbody spectrum.



The background ionization fraction  $\bar{x}_e$  is taken from RECFAST [22]. The effect of the optical depth term in Eq. (32) is only about 1% on the angular-power spectrum.

Assuming purely Compton cooling, the background gas temperature evolves according to [22,23]

$$\dot{\bar{T}}_g + 2\mathcal{H}\bar{T}_g = -\frac{8a\sigma_T\bar{\rho}_\gamma\bar{x}_e}{3m_e c(1+f_{\text{He}}+\bar{x}_e)}(\bar{T}_g - \bar{T}_\gamma), \quad (33)$$

where  $\sigma_T$  is the Thomson scattering cross section,  $f_{\text{He}} = n_{\text{He}}/n_H$ , and we have ignored the very small effect of 21 cm radiation. The perturbations evolve with

$$\begin{aligned} \dot{\Delta}_{T_g} &= 2\dot{\phi} - \frac{2}{3}k\nu - \frac{8a\sigma_T\bar{\rho}_\gamma\bar{x}_e}{3m_e c(1+f_{\text{He}}+\bar{x}_e)} \left[ \left(1 - \frac{\bar{T}_\gamma}{\bar{T}_g}\right) \right. \\ &\quad \times \left. \left\{ 4\Delta_{T_\gamma} + \psi + \frac{\Delta_{x_e}}{1+\bar{x}_e/(1+f_{\text{He}})} \right\} \right. \\ &\quad \left. + \frac{\bar{T}_\gamma}{\bar{T}_g}(\Delta_{T_g} - \Delta_{T_\gamma}) \right], \quad (34) \end{aligned}$$

where we neglected helium fraction perturbations. Note that, although the direct contribution of  $\Delta_{x_e}$  in Eq. (32) is small, the indirect effect on the evolution of  $\Delta_{T_g}$  can be significant. The equations for approximately calculating  $\Delta_{x_e}$  are given in Appendix D. An overdensity has positive  $\Delta_{T_g}$  but recombines more fully than the background and hence has negative  $\Delta_{x_e}$ ; the additional effect of the ionization fraction perturbation is therefore to reduce the coupling to the CMB and hence slightly decrease the spin temperature. Typical transfer functions for the perturbations are shown in Fig. 4 in the synchronous gauge that we use for numerical work. The Newtonian-gauge functions differ on superhorizon scales ( $k \lesssim 10^{-3} \text{ Mpc}^{-1}$  at  $z = 50$ ). For example, the CDM transfer function flattens to  $\approx 6/5$  on large scales.

Assuming an ideal gas, the gas pressure perturbation  $\delta p/\bar{\rho}_g = c_s^2\Delta_g$  is given by

$$\begin{aligned} c_s^2\Delta_g &= \frac{k_B\bar{T}_g}{\mu}(\Delta_g + \Delta_{T_g}) \\ &\approx \frac{k_B\bar{T}_g}{m_p}([1+\bar{x}_e](1-Y_{\text{He}}) \\ &\quad + Y_{\text{He}}m_p/m_{\text{He}})(\Delta_g + \Delta_{T_g}), \quad (35) \end{aligned}$$

where  $\mu$  is the mean particle mass and  $Y_{\text{He}}$  is the mass fraction in helium. This result must be used on scales where the baryon pressure is important [9]. Note that on these scales there may also be additional effects due to CDM decoupling [24] that we neglect here. The evolution of the gas and spin-temperature perturbations is shown in Fig. 3 for two different scales, along with the relative evolution of the baryon and CDM perturbations. Again, these are in the synchronous gauge but they are very

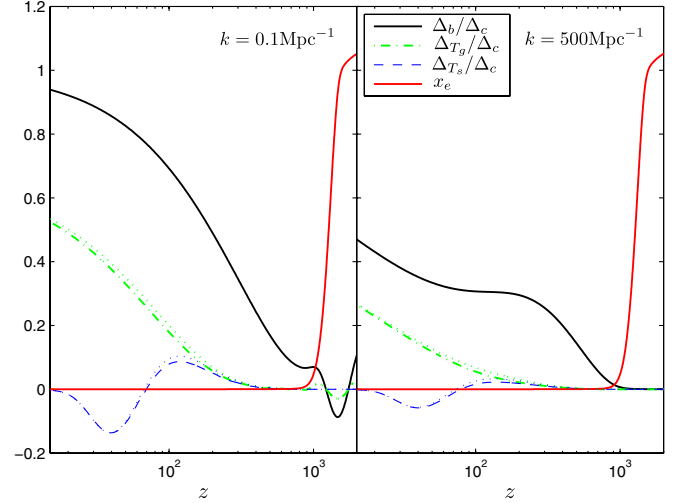


FIG. 3 (color online). Evolution of the fractional baryon, matter, and spin-temperature perturbations as a fraction of the CDM density perturbation. The left figure is for a  $k = 0.1 \text{ Mpc}^{-1}$  mode, the right figure shows the effect of baryon pressure at  $k = 500 \text{ Mpc}^{-1}$ . The dotted lines show the equivalent results neglecting ionization fraction perturbations. In both cases the baryon perturbation is significantly less than the CDM perturbation at all relevant redshifts. There is no reionization.

similar to the Newtonian-gauge perturbations since both wavelengths are subhorizon for the redshift range plotted.

To evaluate the sources for reionization Thomson scattering we need to evolve the multipole equation,

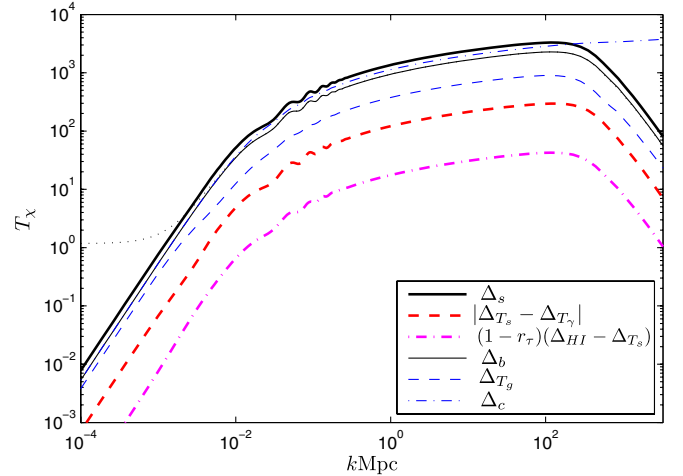


FIG. 4 (color online). Transfer function for monopole source at redshift  $z = 50$  given unit initial curvature perturbation, compared to other relevant perturbations. The perturbations are numerically evaluated in the synchronous gauge. The Newtonian-gauge fluctuations equal those in the synchronous gauge well inside the horizon ( $k \gg 10^{-3} \text{ Mpc}^{-1}$ ). On large scales, the Newtonian-gauge  $\Delta_b$  flattens out at  $\approx 6/5$  times the primordial curvature perturbation, as shown by the dotted curve. The spin-temperature perturbation is negative at  $z = 50$  (see Fig. 3).

$$\begin{aligned}
\dot{F}_l + \frac{k}{2l+1} [(l+1)F_{l+1} - lF_{l-1}] + \delta_{l0}\epsilon\partial_\epsilon\bar{f}\dot{\phi} + \frac{\delta_{l1}}{3}\epsilon\partial_\epsilon\bar{f}k\psi \\
= a\bar{\rho}_s \left[ \delta_{l0}(\Delta_s + \psi) - \frac{\delta_{l1}}{3} \left( \frac{\bar{T}_\gamma}{\bar{T}_s - \bar{T}_\gamma} \right) (v_\gamma - v) - (1 - \delta_{l0} - \delta_{l1}) \frac{\bar{T}_\gamma}{\bar{T}_s - \bar{T}_\gamma} \Theta_l \right] \delta(\epsilon/a - E_{21}) \\
- \dot{\tau}_c \left[ (\delta_{l0} - 1)F_l - \frac{\delta_{l1}}{3} v\epsilon\partial_\epsilon\bar{f} + \delta_{l2} \frac{F_2}{10} \right] - \dot{\tau} [F_l + \delta_{l0}(\Delta_{HI} - \Delta_{T_s} + \psi)\bar{f}] - \delta_{l1} \frac{v}{3} (\partial_\epsilon[\epsilon\bar{f}] + \dot{\tau}\epsilon\partial_\epsilon\bar{f}). \quad (36)
\end{aligned}$$

Neglecting the self-absorption terms involving  $\dot{\tau}$  this is straightforward to propagate numerically after integration over a window function in frequency to remove the delta-functions, as discussed further in Appendix B. Other perturbed quantities and the photon temperature and polarization multipoles evolve according to standard results as implemented in the numerical codes CMBFAST and CAMB [25–28].

## V. APPROXIMATE RESULTS

The general form of the equal-redshift angular-power spectra can easily be understood. On superhorizon scales, the potential  $\phi$  is close to scale invariant and constant, so (from the Poisson equation in the comoving gauge)  $\Delta_c \sim k^2/\mathcal{H}^2\phi$ . Hence, on entering the horizon ( $k \sim \mathcal{H}$ ) the matter perturbations are of order of the potential,  $\Delta_c \sim \phi$ . During radiation domination photon pressure prevents gravitational collapse: the perturbations only grow logarithmically. As a result the spectrum of  $\Delta_c$  is approximately scale invariant on subhorizon scales at matter-radiation equality, though superhorizon scales still have  $\Delta_c \sim k^2/\mathcal{H}^2\phi$ . During matter domination, the potential remains constant and  $\Delta_c$  grows at the same rate independent of  $k$  on all scales where baryon pressure can be neglected. The result is that an initially scale-invariant potential gives comoving-gauge CDM perturbations with an amplitude scaling as  $k^2$  on large scales and growing logarithmically with  $k$  on small scales. The Newtonian-gauge CDM perturbation equals that in the comoving gauge well inside the horizon, but on larger scales the Newtonian gauge  $\Delta_c \approx -2\phi$  in matter domination.

For superhorizon modes, the dominant 21 cm sources in the Newtonian gauge are

$$\delta f(\eta_A, \mathbf{x}_A, \boldsymbol{\epsilon}, \hat{\mathbf{n}}) \approx \bar{f}(\boldsymbol{\epsilon})(\Delta_s + \psi) - \bar{f}_{,\text{ln}\boldsymbol{\epsilon}}(\boldsymbol{\epsilon})\psi, \quad (37)$$

where we have ignored reionization and the effect of non-zero 21 cm optical depth. The source  $\Delta_s$  scales with the hydrogen perturbation  $\Delta_{HI}$ . After recombination almost all the atoms are neutral and  $\Delta_{HI} = \Delta_b$ . On scales above the baryon sound horizon at recombination, the baryons fall into the CDM potential wells on a Hubble time scale, so  $\Delta_b$  evolves to follow  $\Delta_c$ . Note that, although  $\Delta_b$  qualitatively follows  $\Delta_c$  well after recombination, the difference can be tens of percent on all subhorizon scales at high redshift. On very small scales growth of  $\Delta_b$  is suppressed once the

perturbation reaches pressure support. The Newtonian-gauge 21 cm sources thus have a scale-invariant amplitude on superhorizon scales, scale as  $k^2$  for subhorizon modes that entered the horizon after matter-radiation equality, are growing logarithmically on small scales, and are suppressed on very small scales where  $c_s^2 k^2/\mathcal{H}^2 \geq 1$  at recombination. This behavior can be seen in Fig. 4.

On small scales the fractional source fluctuation is of the order of the CDM density perturbation,  $\Delta_s \sim (k/\mathcal{H})^2\phi$ , and the velocity is given by  $v \sim (\mathcal{H}/k)\Delta_c$ . For small scales with  $k \gg \mathcal{H}$ , the line-of-sight result in Eq. (25) is therefore dominated by the monopole and redshift distortion effects, giving the usual approximation for the 21 cm source when we neglect self-absorption effects (take  $\tau_\epsilon = 0$ ):

$$F_l(\eta_A, \mathbf{x}_A, \boldsymbol{\epsilon}, k) \approx e^{-\tau_\epsilon} \bar{f}(\boldsymbol{\epsilon}) \left[ \Delta_s j_l(k\chi_\epsilon) + \frac{kv}{\mathcal{H}} j_l''(k\chi_\epsilon) \right]. \quad (38)$$

The fractional angular-power spectrum for one redshift shell is then

$$\begin{aligned}
C_l(z, z) \approx 4\pi e^{-2\tau(z)} \int d\text{ln}k \{ \mathcal{P}_{\Delta_s}(k, z) [j_l(k\chi(z))]^2 \\
+ 2\mathcal{P}_{v\Delta_s}(k, z) j_l(k\chi(z)) j_l''(k\chi(z)) \\
+ \mathcal{P}_{vv}(k, z) [j_l''(k\chi(z))]^2 \}, \quad (39)
\end{aligned}$$

where  $\mathcal{P}_{\Delta_s}$ ,  $\mathcal{P}_v$ , and  $\mathcal{P}_{v\Delta_s}$  are the power spectra of  $\Delta_s$ ,  $kv/\mathcal{H}$ , and their cross correlation.<sup>1</sup> For  $k\chi$  several oscillations larger than  $l$ , and smooth power spectra, we can replace the products of the rapidly oscillation Bessel functions with their approximate smooth averages from Appendix E.

One might expect the low- $l$  21 cm fluctuations to be dominated by the superhorizon scale, post-Newtonian fluctuations at scale  $k = l/\chi$ . This is not correct since small-scale fluctuations, with amplitude growing rapidly with scale as  $k^2$ , couple to  $l < k\chi$  through the oscillatory tails of the spherical Bessel functions. The net effect is that, for all  $l$  and a single source plane, the dominant contribution is from modes that are inside the horizon. At low  $l$ , the  $C_l$  integral of Eq. (26) is therefore dominated by much smaller scales, with  $k \gg l/\chi$ . In this limit the Bessel functions can

<sup>1</sup>We define power spectra so that  $\langle \Delta(x)^2 \rangle = \int d\text{ln}k \mathcal{P}(k)$ .

be approximated with the asymptotic result  $j_l(k\chi) \sim \cos[k\chi - (l+1)\pi/2]/(k\chi)$ . Since the power spectrum is quite smooth, we can then average over oscillations using  $\langle |j_l(k\chi)|^2 \rangle \sim 1/[2(k\chi)^2]$ . We can similarly remove oscillating terms in the second derivative term. Hence on large scales, keeping only the monopole source and redshift distortions and assuming a narrow redshift window, the dimensionless fractional power spectrum is

$$C_l(z, z) \sim 4\pi e^{-2\tau_c} \int d \ln k \frac{\mathcal{P}_s(k, z)}{2k^2 \chi(z)^2}, \quad (40)$$

where  $\mathcal{P}_s(k, z)$  is the power spectrum of  $\Delta_s - kv/\mathcal{H}$  at redshift  $z$  [conformal distance  $\chi(z)$ ]. Since this is independent of  $l$  it corresponds to a white-noise spectrum. The intrinsic fluctuations on a scale  $k = l/\chi$  are hidden beneath random variations in the large-scale distribution of much smaller perturbations. This is a generic feature of the 21 cm angular-power spectrum that is also true after the dark ages [6].

Scales inside the horizon at matter-radiation equality have an approximately scale-invariant spectrum (grow logarithmically with  $k$ ). This causes the 21 cm power spectrum to flatten out. First consider the case where the window function is sharp,  $\Delta\chi/\chi \ll 1/l$ , so the source is from a single redshift. For monopole and velocity sources with power-law spectra, the result for  $C_l$  from Eq. (39) can be obtained analytically using a result for integrating products of spherical Bessel functions quoted in Appendix E. In particular, taking the power spectrum to be approximately constant on small scales, we can approximate the dimensionless fractional power spectrum as

$$\begin{aligned} \frac{l(l+1)}{2\pi} C_l(z, z) \sim e^{-2\tau_c} \left[ \mathcal{P}_{\Delta_s}(\pi l/2\chi(z), z) \right. \\ \left. - \frac{2}{3} \mathcal{P}_{v\Delta_s}(3\pi l/4\chi(z), z) \right. \\ \left. + \frac{1}{5} \mathcal{P}_v(15\pi l/16\chi(z), z) \right]. \quad (41) \end{aligned}$$

The numerical factors are consistent with the angular average of Eq. (21). Since the small-scale spectrum actually grows logarithmically, the power spectra in Eq. (41) are approximated by their values at the mean position of the corresponding window function. The Bessel functions are skewed to  $k > l/\chi$  so that the mean of a  $[j_l(r)]^2/r$  window is at  $r = l(l+1)\pi/(2l+1) \sim \pi l/2$ . The velocity and cross-power window functions probe even smaller scales  $\sim 15\pi l/16$  and  $\sim 3\pi l/4$ , respectively. Equation (41) is accurate at the 10% level from the end of the baryon oscillations to the baryon damping scale at  $l \sim 10^6$ . The power is overestimated because the underlying power spectra are only growing logarithmically rather than linearly. In the (crude) approximation that  $\Delta_s \sim \Delta_b \sim \Delta_c$  so that  $kv/\mathcal{H} \sim kv_c/\mathcal{H} \sim -\Delta_s$ , and taking  $\mathcal{P}(k)$  to be constant, we have

$$\frac{l(l+1)}{2\pi} C_l(z, z) \sim \frac{28}{15} e^{-2\tau_c} \mathcal{P}_{\Delta_s}(k, z). \quad (42)$$

Though not very accurate this result shows the importance of redshift distortions: it is  $\sim 28/15 \sim 1.87$  times larger than the equivalent approximate result neglecting them.

On scales where the wavelength is much smaller than the redshift bin width,  $l \gtrsim \chi/\Delta\chi$ , redshift-distortion effects average out and we can instead use the Limber approximation:

$$\begin{aligned} C_l(z, z) \approx e^{-2\tau_c} \frac{2\pi^2}{l^3} \int_0^{\chi_*} \chi d\chi W(\chi)^2 \\ \times \mathcal{P}_{\Delta_s}(k = l/\chi(z); \eta_0 - \chi(z)), \quad (43) \end{aligned}$$

where  $\chi_*$  is the far end of the window function  $W(\chi)$ . Since the source power spectrum is nearly scale invariant,  $C_l$  therefore scales approximately as  $1/l^3$ . In other words  $l^2 C_l$  is approximately constant with an additional  $1/l$  suppression due to line-of-sight averaging through the window. If  $W$  is a Gaussian of width  $\sigma$ , the line-of-sight averaging causes the overall amplitude to scale approximately as  $1/\sigma$ . The Limber approximation can in fact be used for numerical calculation on scales with  $l \gg \chi/\Delta\chi$  where it becomes accurate.

On very small scales where modes are inside the baryon sound horizon at recombination,  $kc_s(\eta_*)\eta_* \gtrsim 1$ , the baryon pressure becomes important and  $\Delta_H$  differs significantly from  $\Delta_c$  even at late times. We discuss approximate analytic solutions for the evolution of  $\Delta_b$  in Appendix A. In the small-scale limit where  $k^2 c_s^2 \gg \mathcal{H}^2$ , the pressure and gravitational forces approximately balance, and  $\Delta_b/\Delta_c \sim \mathcal{H}^2/(k^2 c_s^2)$ . Since  $\Delta_c$  is roughly scale invariant, and neglecting the effect of the baryon pressure on the CDM evolution, this implies  $l^2 C_l \propto 1/l^4$ , giving a characteristic sharp falloff in power on very small scales (there is an additional power of  $1/l$  for window-function line-of-sight averaging). Note the observations on such small scales are unlikely to be possible at high redshift over most of the sky due to scattering by turbulent galactic and solar-system plasma [29]. The nonzero linewidth also becomes important on these scales, so our results in the approximation of a monochromatic source will overestimate the power.

## VI. NUMERICAL RESULTS

For our numerical results we assume a standard concordance flat adiabatic CDM ( $\Omega_c h^2 = 0.104$ ) model with a constant primordial spectral index ( $n_s = 0.95$ ) and optical depth to Thomson scattering  $\tau = 0.09$ . We take baryon density  $\Omega_b h^2 = 0.022$ , Hubble parameter  $73 \text{ km s}^{-1} \text{ Mpc}^{-1}$ , and initial curvature perturbation power on  $0.05 \text{ Mpc}^{-1}$  scales  $A_s = 2.04 \times 10^{-9}$ . We neglect the neutrino masses, which do not have a large effect for source planes at high enough redshift that the neutrinos

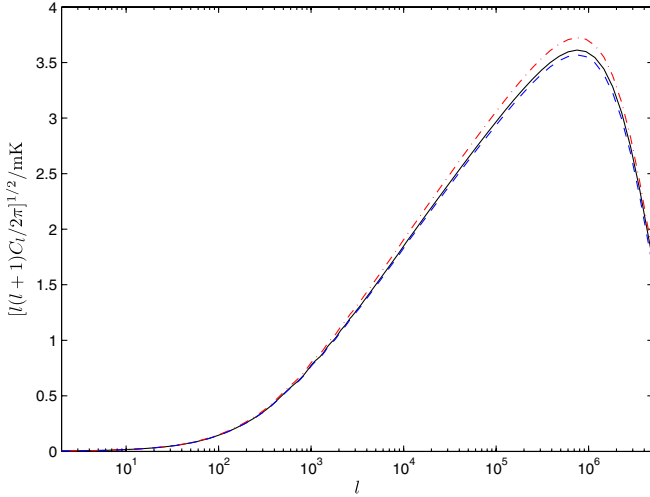


FIG. 5 (color online). The effect of perturbations to the optical depth and ionization fraction on the 21 cm power spectrum at  $z = 50$  with a sharp window function. The solid line shows our main result, the dash-dotted line is the larger result using the a zeroth-order expansion in  $\tau_e$ , the dashed line is the lower result if the effect of ionization fraction perturbations on the gas temperature evolution is neglected. The fractional change in the spectrum is roughly the same on all scales where baryon pressure is negligible.

are still relativistic. We take our window function to be a Gaussian of width  $\Delta\nu$  in frequency over the observed brightness.

Figure 5 shows the effect on the angular-power spectrum of allowing for self-absorption and ionization fraction perturbations. The finite nonzero optical depth lowers the amplitude both because the background signal is lower and because the optical depth from an overdensity is higher than from the background; each effect is about  $\tau_e/2 \sim 1.5\%$  in amplitude, giving an overall suppression of  $\sim 6\%$  in power. Ionization fraction perturbations increase the power by about 2% on all scales: overdensities recombine more fully and hence have less Compton coupling to the CMB and hence lower spin temperature. These effects are important on all scales and should be included in any accurate calculation, though note that they are comparable to other effects that we have neglected because of the simple velocity-independent spin-temperature approximation (see Ref. [19]).

On small scales the post-Newtonian and extra velocity terms can be neglected to good accuracy. On large scales they can be more important. In Fig. 6 we show the contribution of the autovariance of various terms to the total large-scale power spectrum at a given redshift. As expected, the dominant contributions are still from the mono-

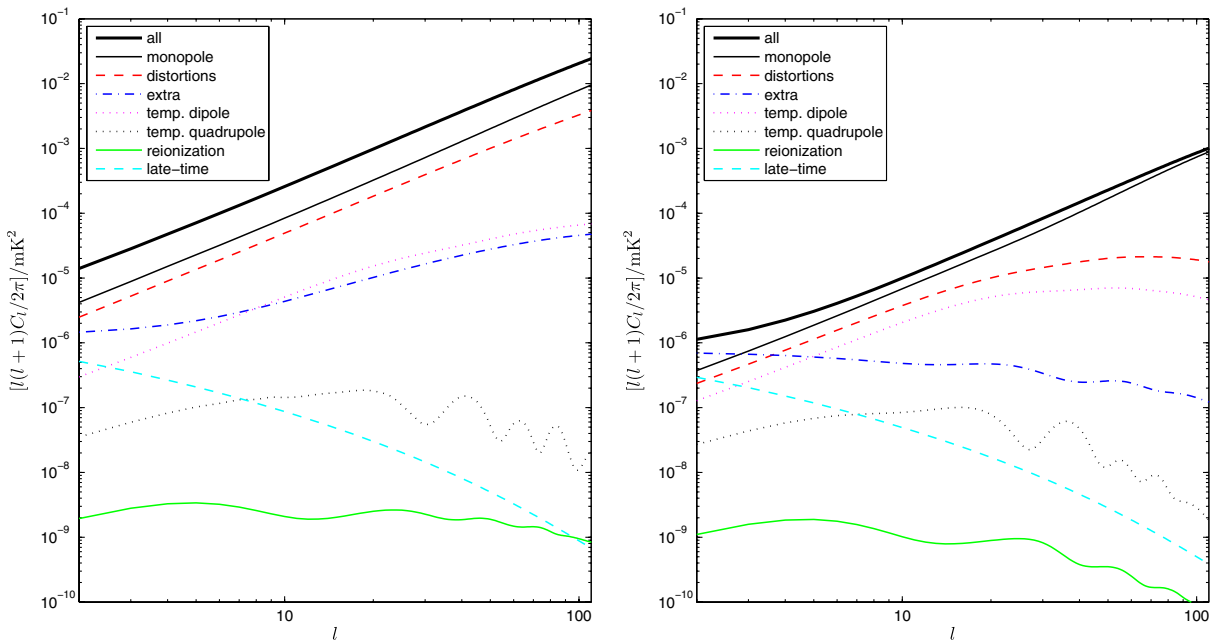


FIG. 6 (color online). Autopower spectra for the various terms in the large-scale 21 cm power spectrum. Left: narrow window function at  $z = 50$  with  $\Delta\nu = 0.01$  MHz ( $T_b = -26$  mK); Right: broad window function at  $z = 40$  with  $\Delta\nu = 5$  MHz ( $T_b = -15$  mK,  $\sigma_z \sim 6$ ). Terms are calculated in the synchronous gauge, and “extra” includes all effects not included in other curves; standard redshift distortions are defined here by the second term in Eq. (38). The late-time curve is the ISW contribution from line-of-sight redshifting. The reionization curve is the result from sources at reionization, the other curves include the main  $e^{-2\tau_e}$  damping effect. The standard calculation includes only monopole and redshift-distortion terms; the difference from the full result is  $\sim 1\%$  at  $l \lesssim 50$  growing to a few percent at low  $l$  for the narrow window function. For the broad window function that averages down small-scale power extra terms change the total by  $\geq 1\%$  at  $l < 100$  (growing to  $\sim 40\%$  at low  $l$ ). Note that the total spectrum is not just the sum of the other autocorrelation terms since it also includes all cross terms.



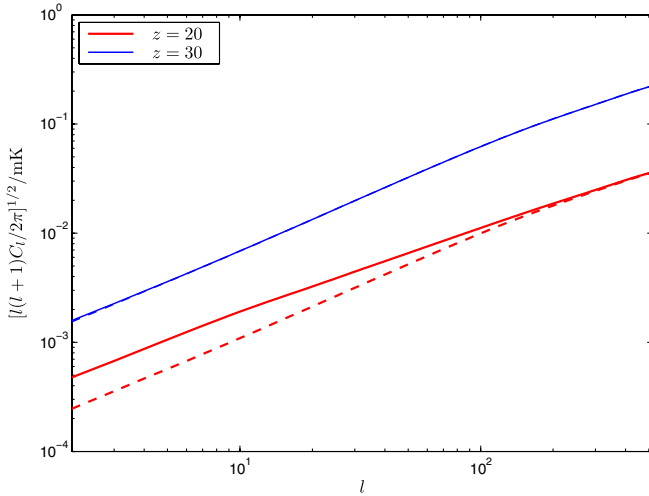


FIG. 7 (color online). The large-scale 21 cm power spectrum at  $z = 20$  and  $z = 30$  ( $\Delta\nu = 0.01$  MHz) if there were no Lyman- $\alpha$  sources, shock heating, minihaloes, or other nonlinear effects. Solid lines are the full linear result, dashed lines include only monopole and redshift-distortion sources. The difference is dominated by the baryon-photon velocity term.

pole source fluctuations and redshift distortions.<sup>2</sup> Except on very large scales the next most important term is from the CMB dipole in the rest frame of the gas, which gives percent-level contribution at  $l < 50$  for the redshift shown here, but is negligible on much smaller scales.<sup>3</sup> At ( $l < 100$ ) the contribution from the potential and other velocity terms is also not entirely negligible. The contributions from the CMB temperature anisotropy above the dipole, and reionization rescattering sources, are completely negligible on all scales. At lower redshifts the background signal becomes smaller, and the relative importance of the terms changes. The background signal depends on  $\bar{T}_s - \bar{T}_\gamma$ , but some of the perturbation sources depend only on the 21 cm optical depth and are nonzero even when the spin temperature is equal to the CMB temperature. As an extreme example, Fig. 7 shows the relatively large contribution from the photon-baryon dipole at  $z = 20$  on large scales if there were no additional sources from nonlinear structures.

Note that just because something does not show up in a narrow frequency window autopower spectrum at a given redshift does not mean that it is necessarily negligible. The correlation between source planes at a given  $l$  falls off very rapidly once the plane separation is greater than character-

<sup>2</sup>Note that at the percent level it is important to use the baryon rather than CDM velocity when calculating the redshift distortions.

<sup>3</sup>Note that although the CMB dipole signal has only a small effect on the dark-age 21 cm power spectrum, it may make a larger contribution to the correlation with other sources, for example the cross correlation with the CMB temperature during reionization (cf. Ref. [30]).

istic perturbation size  $\chi/l$ . Extra information may therefore be available in the cross-power spectra, particularly about small large-scale signals that are correlated between redshift bins. The effect of different frequency window functions is shown in Fig. 8. Here the baryon oscillations only show up when the window is wide enough to damp down the large smaller-scale fluctuations so that the power on baryon oscillation scales is not dominated by contributions from smaller scales. When narrow frequency windows are used this information is hidden in the cross-correlation structure of the different source planes.

The white-noise signal on large scales can be reduced by averaging over many redshift slices. Figure 6 shows the relative importance of the various terms on large scales when a broad redshift window function is used. Redshift distortions from scales smaller than the bin width are suppressed, and the large-scale white-noise monopole signal is reduced because of the line-of-sight averaging of small-scale power. The relative importance of the additional terms is therefore larger. This raises the question of whether the large-scale 21 cm signal can be useful, for example, to learn about large-scale power or as a source for the integrated Sachs-Wolfe effect (ISW). There are two main problems. First, a very broad window function is required to make the extra terms comparable to the monopole source, and residual monopole and redshift-distortion signals will generally dominate. Second, since the dark-age redshift shells are  $\geq 3/4$  of the comoving distance to the last scattering surface, large-angle correlations, such as those due to Sachs-Wolfe potential redshifting, will be strongly correlated between redshift slices and correlated with the large-scale CMB. As an averaged source plane for

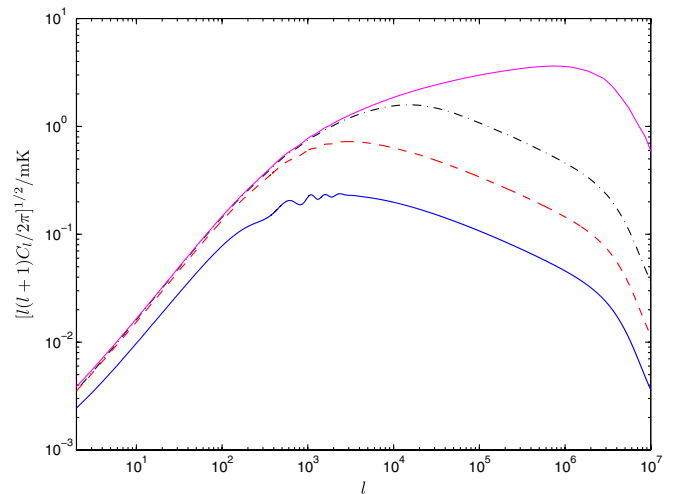


FIG. 8 (color online). The 21 cm power spectrum at  $z = 50$  for  $\Delta\nu = \{1, 0.1, 0.01, 0\}$  MHz (bottom to top). Large widths suppress the redshift-distortion contribution and allow the baryon oscillations to be seen. All show characteristic damping due to line-of-sight averaging over the bin width at  $l \geq \chi/\Delta\chi$ , and the effect of baryon pressure at  $l \geq 5 \times 10^6$ .



the ISW the 21 cm signal therefore has at least as much large-scale “noise” from other sources as the CMB and hence offers little extra information.

Decorrelation with source plane separation is a powerful way to try and separate intrinsic and foreground signals due to the much smoother signal (as a function of frequency) expected from most foregrounds [7,31]. Detection of small nonforeground cross correlations is therefore particularly challenging.

## VII. POLARIZATION

A quadrupole anisotropy in the 21 cm signal at reionization can generate polarization by Thomson scattering [32]. The signal is expected to be very small, but perhaps worth considering as polarization may be very useful to help with foreground cleaning of scalar modes. In principle, the tensor mode signal can also be used as a cross-check on CMB temperature and polarization constraints on models of inflation.

Following standard methods [33,34], it is straightforward to modify our scalar equations to include polarization in order to calculate the E-mode (gradientlike) spectrum generated at reionization. For our idealized analysis we neglect any effects due to magnetic fields, anisotropy of the

hydrogen triplet state distribution, and inhomogeneity of reionization. Typical numerical results are shown in Fig. 9.

Gravitational waves (tensor modes) are known to be subdominant to the scalar modes, but can also source anisotropies by their anisotropic shearing. There are two mechanisms. First, the metric shear can directly change the 21 cm photon frequency along the line of sight, which distorts the emission shell in much the same way as the redshift distortions and line-of-sight effects do for the scale modes. Second, the CMB temperature at absorption will be anisotropic due to gravitational waves between the absorber and the last scattering surface: this causes an anisotropy in the 21 cm absorption. At reionization, the quadrupole component of these anisotropies source both E and B polarization. The signal is a small fraction of the blackbody tensor signal because the optical depth for 21 cm emission is only  $\sim 0.02$ . Note that since there is no intrinsic 21 cm polarization before reionization, the lensing-induced 21 cm B-modes are much smaller.

## VIII. NONLINEAR EVOLUTION

Although the dark-age perturbations are quite small, nonlinear effects can still be important. This is clear from Fig. 4, where the perturbation amplitude on Jeans’ scales at  $z = 50$  corresponds to density perturbations of order 10%. We shall estimate the effect of nonlinear evolution using Newtonian perturbation theory in the approximation that vorticity and decaying modes are unimportant. The result should be quite accurate for the dark matter density as perturbation theory gives good results in the mildly nonlinear regime. Assuming an initially Gaussian field, one might expect the nonlinear contribution to the power spectrum to be of order  $|\Delta_c|^4$ , corresponding to a correction of about 1%. However, on very small scales, there are many larger scale  $k$ -modes that contribute to the local density, giving a total effect from all mode couplings that is significantly larger than the simple estimate.

For our approximate analysis, we focus on the CDM perturbations during matter domination, neglecting any effect due to the baryons. The first nonlinear contribution to the power spectrum comes from two terms,  $\mathcal{P}_{22}$  coming from the square of the second-order perturbation, and  $\mathcal{P}_{13}$  coming from the cross term between the first- and third-order perturbations. We give the results for the CDM density, velocity, and cross-correlation power spectra in Appendix F; see Fig. 10 for typical numerical results.

To calculate the effect of nonlinear evolution on the 21 cm power spectrum, one should really evolve the full coupled baryon, temperature, and CDM equations to third order. This is beyond the scope of this paper. Here we instead make the approximation that the 21 cm monopole source and baryon velocity power spectra have the same fractional contribution from nonlinear evolution as do the CDM power spectra. Using Eq. (39), we then get the results shown in Fig. 11. Nonlinear effects are important at the

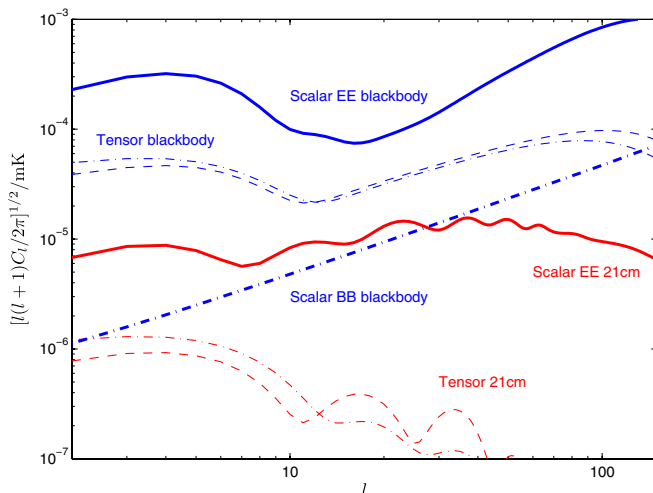


FIG. 9 (color online). The 21 cm polarization power spectra from  $z = 50$  with  $\Delta\nu = 0.01$  MHz. Thick lines show the adiabatic scalar-mode signal, thin lines from  $r \equiv A_T/A_s = 0.1$  scale-invariant tensor modes. For comparison, the intrinsic CMB polarization signals (labeled blackbody) are also plotted: the scalar *EE* blackbody curve is the lensed E-mode polarization from scalar modes and the scalar *BB* blackbody curve is the lens-induced B-mode power; the tensor blackbody curves are the CMB polarization power spectra from gravity waves. For both intrinsic CMB and 21 cm fluctuations, E-mode polarization is shown with solid or dashed lines and B-modes with dash-dotted lines. There are no 21 cm scalar B-modes within our approximations. Reionization is assumed to be fairly sharp with optical depth  $\tau = 0.09$  ( $z_{\text{re}} \sim 12$ ).

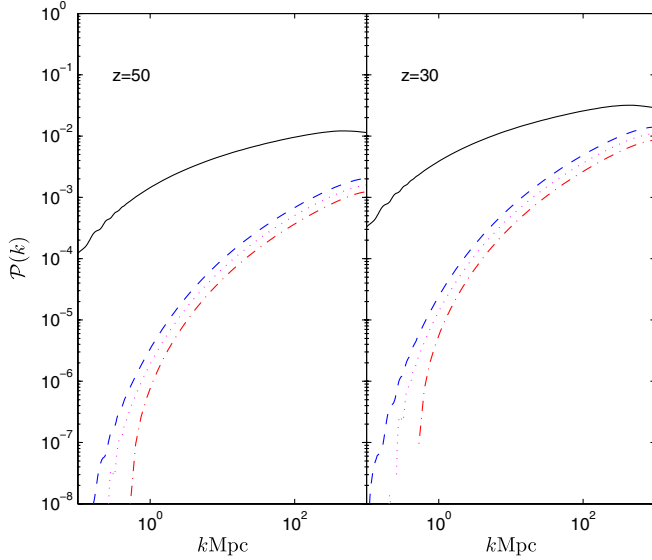


FIG. 10 (color online). Power spectrum of the dark matter  $\mathcal{P}(k)$ , linear result (solid) and approximate second-order terms from Appendix F:  $\mathcal{P}^{\delta\delta}(k)$  (dashed),  $\mathcal{P}^{\nu\nu}(k)$  (dot-dashed),  $-\mathcal{P}^{\nu\delta}(k)$  (dotted). On large scales the second-order contributions become negative (not shown).

few-percent level on small scales even at redshift  $z \sim 50$ . At redshift  $z \sim 30$  there is a  $\sim 10\%$  correction to the power spectrum at  $l \sim 10^5$ . A more accurate analysis at redshift  $z \sim 30$  may need to account for gas shock heating, minihalos, or even rare first sources (see e.g. Ref. [3] and references therein).

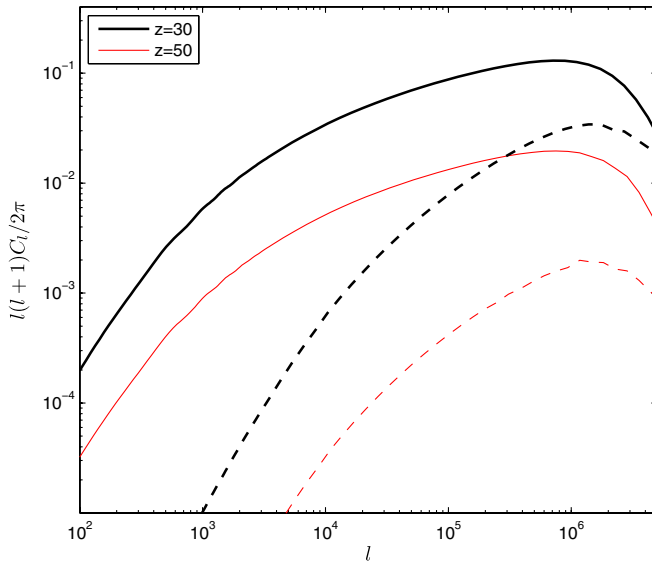


FIG. 11 (color online). The linear 21 cm angular-power spectrum at  $z = 30$  and  $z = 50$  (solid lines), and the approximate higher-order correction from nonlinear evolution (dashed lines). Window functions are taken to be sharp ( $\Delta\nu = 0$ ).

## IX. LENSING

The line emission spectrum is not affected by lensing at first order. However, perturbations along the line of sight can produce a non-negligible higher-order effect. The effect on the two- and three-dimensional power spectra has been analyzed in detail in Ref. [40]. Lensing acts rather like a convolution of the angular-power spectrum with the deflection-angle power spectrum. Since the 21 cm power spectrum is rather smooth, the effect is significantly smaller than on the CMB. Nonetheless the baryon wiggles can be smoothed at well above the cosmic variance level. Here we note a simple, nonperturbative approach to calculating the effect on the angular-power spectrum. This is based on the lensed correlation function method often applied to the CMB temperature and polarization [41–43].

Since the lensing field is nearly linear, the effect is well described in terms of the lensing deflection-angle power spectrum  $C_l^\alpha(z, z')$ . In linear theory this is given in terms of the primordial power spectrum  $\mathcal{P}_{\mathcal{R}}(k)$  and transfer functions  $T_\Psi(k; \eta)$  for the Weyl potential,  $\Psi \equiv (\phi + \psi)/2$ , by (see e.g. Ref. [43])

$$C_l^\alpha(z, z') = 16\pi l(l+1) \int \frac{dk}{k} \mathcal{P}_{\mathcal{R}}(k) \times \left[ \int_0^{\chi(z)} d\chi T_\Psi(k; \eta_0 - \chi) j_l(k\chi) \left( \frac{\chi(z) - \chi}{\chi(z)\chi} \right) \right] \times \left[ \int_0^{\chi(z')} d\chi' T_\Psi(k; \eta_0 - \chi') j_l(k\chi') \left( \frac{\chi(z') - \chi'}{\chi(z')\chi'} \right) \right], \quad (44)$$

where  $\chi(z)$  is the conformal distance to the window at redshift  $z$ . We assume the window function is narrow compared to the distance so that the lensed sources can be approximated as a single source plane. For nearby bins the terms in square brackets are approximately equal.

In terms of  $C_l^\alpha(z, z')$  and the unlensed spectrum  $C_l(z, z')$ , the lensed power spectrum is given to very good accuracy by [43]

$$\tilde{C}_l(z, z') \approx \sum_l \frac{2l+1}{2} C_l(z, z') \int_{-1}^1 d \cos \beta d_{00}^l(\beta) \times e^{-l(l+1)\sigma^2(\beta)/2} \sum_{n=-l}^l I_n[l(l+1)] \times C_{gl,2}(\beta)/2] d_{n-n}^l(\beta), \quad (45)$$

where  $I_n$  is a modified Bessel function,  $d_{mn}^l$  are reduced Wigner functions,  $\sigma^2(\beta) \equiv C_{gl}(0) - C_{gl}(\beta)$ , and

$$C_{gl,2}(\beta) \equiv \sum_l \frac{2l+1}{4\pi} C_l^\alpha(z, z') d_{-11}^l(\beta), \quad (46)$$

$$C_{gl}(\beta) \equiv \sum_l \frac{2l+1}{4\pi} C_l^\alpha(z, z') d_{11}^l(\beta).$$

The sum over  $n$  is dominated by the lowest terms with

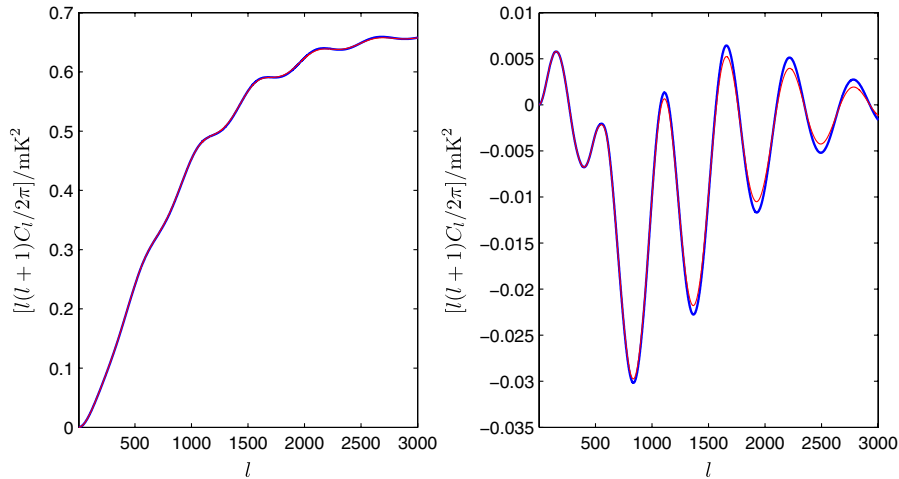


FIG. 12 (color online). The 21 cm power spectrum for bins at  $z = 50$  and  $z = 52$  ( $\Delta\nu = 0.1$  MHz), with lensing (thin lines) and without lensing (thick lines). The left figure shows  $C_l(z, z)$ , the right figure shows the small but non-negligible cross correlation.

$|n| \approx 0$ . For a  $\Delta\nu = 1$  MHz window at  $z = 50$ , the lensing-induced smoothing of the baryon oscillations can be nearly a percent, but elsewhere the effect on the angular-power spectrum is generally very small because it is smooth on the scale of the width of the deflection-angle power spectrum ( $\Delta l \sim 100$ ). Figure 12 shows the significant smoothing effect on the cross-correlation power spectrum on the scale of the baryon oscillations.

In addition to the small effect on the power spectrum calculated here and in Ref. [40], lensing also makes the distribution non-Gaussian. Combined with tomographic information this can be used for lensing reconstruction [44–46].

## X. OTHER NONLINEAR EFFECTS

On small scales much larger than the linewidth, the nonlinear angular distribution can be obtained from integrating Eq. (14). In the Newtonian approximation, neglecting self-absorption and lensing, and dropping small  $\hat{\mathbf{n}} \cdot \mathbf{v}$  terms that are unimportant on small scales, we have the approximate nonlinear result,

$$f(\hat{\mathbf{n}}, z) \approx e^{-\tau_c} \sum_{\chi'} \frac{(1 + \Delta_s) \bar{\rho}_s}{1 + (\hat{\mathbf{n}} \cdot \partial \mathbf{v} / \partial \chi) / \mathcal{H}} \Big|_{\chi'}, \quad (47)$$

where  $\chi'$  are displaced positions satisfying  $\chi' = \chi(z) - \hat{\mathbf{n}} \cdot \mathbf{v}(\chi') / \mathcal{H}$ . In the linear approximation we used  $\Delta_s(\chi') = \Delta_s(\chi)$ , however this will not be a good approximation if the Doppler displacement is comparable to the scale of the perturbation. The root-mean square velocity is around  $3 \times 10^{-4}$  at redshift 50, corresponding to a displacement of  $\sim 0.3$  Mpc, and hence suggesting that nonlinear Doppler displacement effects may become large at  $k \sim 10 \text{ Mpc}^{-1}$ . However, the small-scale *power spectrum* will be unchanged under small bulk radial displacements:

the spectrum at wave number  $k$  is only really sensitive to the *difference* in the radial displacement over a distance comparable to  $1/k$ . Since the velocity power spectrum falls with scale, the effect is much smaller than indicated by the above estimate. The displacement on scale  $k$  is given by  $\delta\chi \sim \hat{\mathbf{n}} \cdot \mathbf{v} / \mathcal{H} \sim \Delta_c / k$ , and thus  $k\delta\chi$  will only become large on scales where  $\Delta_c$  does. Coupling to smaller scales will give an effective velocity dispersion similar to a scale-dependent thermal line broadening, and will tend to reduce the power. Since the velocity power falls with  $k$  this is never a large effect. The total nonlinear effect is therefore likely to be comparable to the estimated contribution from just the nonlinear evolution.

A perturbative analysis using third-order Newtonian perturbation theory is given in Ref. [47]. Since higher-order corrections to  $\Delta_s(\chi')$  are large on small scales, but the correction to the power spectrum is small due to the large coherence length of the displacement, a perturbative treatment will involve delicate cancellations between different independently large terms. A more physical non-perturbative method using the correlation functions (which are insensitive to large-scale bulk displacements) is given in Ref. [38]. A detailed investigation of the effect on the small-scale 21 cm power spectrum is beyond the scope of this paper.

## XI. CONCLUSIONS

The 21 cm signal from the dark ages is potentially a powerful probe of cosmology. We have derived full linear-theory results for the angular-power spectra, and confirmed that, for most purposes, standard approximations including only monopole sources and redshift distortions are accurate at the percent level. However, additional velocity and potential terms can be non-negligible on very large scales, and optical depth and ionization fraction perturbations have a significant percent-level effect on all scales.

Nonlinear evolution can be a many-percent effect on small scales even at high redshift, and gravitational lensing can also be important, though this is easily modeled.

In this paper we have focussed on theoretical issues. The observational problems are formidable, requiring many square kilometers of collection area, low radio noise, and, for high redshifts, getting outside the atmosphere to avoid the opaque ionosphere; see Refs. [3,5,7,48] for further discussion. The additional hurdles to measure the distinctive polarization signal that we calculated, which is below the intrinsic blackbody signal, are quite possibly insurmountable.

The 21 cm spectrum is much more sensitive to the residual ionization fraction after recombination than the CMB temperature: the ionization fraction governs the evolution of the matter temperature which in turn affects the background brightness and the evolution of the perturbations. Current modeling of recombination is probably insufficiently detailed to be able to compute the 21 cm power spectrum to an accuracy of more than a couple of percent as there are a wealth of subtle effects that need to be modeled to calculate hydrogen recombination accurately [49]. As an example of current uncertainties, using the result of Ref. [50] rather than RECFAST [22] for the postrecombination ionization fraction changes the 21 cm brightness temperature at the two-percent level. If future observations are to achieve the  $\sim O(10^{-5})$  accuracy on cosmological parameters that is possible in principle, a very detailed analysis will be required of the full electron, atomic state, and velocity distributions, with all interactions, extending the work of Ref. [19]. Furthermore, even at redshift of 50 the Jeans'-scale density perturbations are already  $O(0.1)$  and nonlinear corrections are important at the many percent level. We estimated this effect with an approximate second-order CDM perturbation theory calculation, however accurate results will require a detailed study of the full baryon-CDM evolution at second and third order or beyond.

Although we have concentrated on the power spectrum from the dark ages, much of our formalism can be adapted straightforwardly to the reionization epoch given models for the background evolution and additional sources. Our numerical code is publicly available [51].

## ACKNOWLEDGMENTS

A.L. thanks Oliver Zahn, Steven Gratton, Ue-Li Pen, and Jeff Peterson for discussion.

## APPENDIX A: BARYON PERTURBATION EVOLUTION

After recombination, Compton scattering has no significant effect on the baryon density evolution and the fractional synchronous gauge baryon perturbation  $\Delta_b$  obeys the equation

$$\begin{aligned} \frac{\partial^2 \Delta_b}{\partial \eta^2} + \mathcal{H} \frac{\partial \Delta_b}{\partial \eta} + k^2 c_s^2 \Delta_b &= 4\pi G a^2 \sum_i (\delta \rho_i + 3\delta p_i) \\ &\approx \frac{3}{2} \mathcal{H}^2 \Delta_m, \end{aligned} \quad (\text{A1})$$

where  $(\rho_b + \rho_c)\Delta_m = \rho_c \Delta_c + \rho_b \Delta_b$  and the second line assumes matter domination. We make the approximation that  $\rho_c \gg \rho_b$  so the baryons have no effect on the CDM evolution and we can use the usual result in matter domination that  $\Delta_m(\eta) = \Delta_c(\eta) = \Delta_c(\eta_*) \eta^2 / \eta_*^2$ . On small scales before recombination the baryons are tightly coupled to the photons and silk damping erases perturbations so that at recombination ( $\eta \sim \eta_*$ ) we have  $\Delta_b(\eta_*) \sim 0$  and  $\dot{\Delta}_b(\eta_*) \sim 0$ . On scales where baryon pressure is irrelevant,  $k c_s / \mathcal{H} \ll 1$  at all times, the solution after recombination is

$$\Delta_b / \Delta_c = 1 - 3 \left( \frac{\eta_*}{\eta} \right)^2 + 2 \left( \frac{\eta_*}{\eta} \right)^3. \quad (\text{A2})$$

On a smaller scale, the baryon pressure is important via the  $k^2 c_s^2$  term in Eq. (A1). The sound speed decays approximately as  $1/\eta$  while Compton scattering couples the gas temperature to the CMB temperature. Once coupling becomes ineffective at  $\eta \sim \eta_a$ , the gas cools adiabatically and  $c_s$  decays as  $1/\eta^2$ . We can solve analytically for the evolution of the baryon perturbation for both limiting behaviors of the sound speed. For  $\eta_* < \eta < \eta_a$ , the result is

$$\begin{aligned} \Delta_b / \Delta_c &= \frac{6}{x^2 + 6} \left[ 1 - \left( \frac{\eta_*}{\eta} \right)^{5/2} \left( \cos[\sqrt{x^2 - 1/4} \ln(\eta/\eta_*)] \right. \right. \\ &\quad \left. \left. + \frac{5}{2\sqrt{x^2 - 1/4}} \sin[\sqrt{x^2 - 1/4} \ln(\eta/\eta_*)] \right) \right], \end{aligned} \quad (\text{A3})$$

where we defined  $x \equiv k c_s(\eta_*) \eta_*$  and assumed  $x > 1/2$ . The analytic continuation of this result to  $x = 0$  agrees with Eq. (A2). A similar result is given in Ref. [52], which also discusses the generalization to non-negligible baryon fraction. On large scales where modes are outside the baryon sound horizon at recombination ( $x \ll 1$ ), the perturbations fall into the CDM potential wells in the order of a Hubble time and  $\Delta_b \rightarrow \Delta_c$ . On small scales the baryon pressure causes the perturbations to oscillate once they reach pressure support. The relative amplitude of the oscillations about the midpoint decays as  $(\eta_*/\eta)^{5/2}$ , so by the time of adiabatic cooling we may neglect this term to  $\sim 10\%$  accuracy. The adiabatic cooling equation is a forced harmonic oscillator equation in  $1/\eta$  with a solution involving sine and cosine integrals that can be written (for  $\eta > \eta_a$ ) as [53]

$$\Delta_b = A \cos(u) + B \sin(u) + \Delta_c \left[ 1 - u^2 \int_0^\infty dt \frac{t e^{-ut}}{t^2 + 1} \right], \quad (\text{A4})$$

where  $u \equiv x\eta_a/\eta = kc_s(\eta)\eta$  and constants  $A$  and  $B$  are defined by the initial conditions. The term in square brackets monotonically decreases from one as  $k$  (and hence  $u$ ) increases, and describes the main effect of the pressure. Smoothly matching to Eq. (A3) (with the oscillation dropped) assuming a sharp transition at  $\eta_a$ , the result can be written as

$$\Delta_b/\Delta_c = 1 - u^2 \int_0^{x-u} \frac{\cos t}{t+u} dt - \frac{u^2}{6+x^2} \left( \cos(u-x) + \frac{4+x^2}{x} \sin(u-x) \right). \quad (\text{A5})$$

As a function of  $k$  this solution reproduces the qualitative falloff in power show in Fig. 4, though the decaying nature of the solution is well hidden in Eq. (A5). The small-scale asymptotic form for  $k \rightarrow \infty$  ( $u, x \gg 1$ ) is

$$\Delta_b/\Delta_c = \frac{6}{u^2} - 12 \frac{u^2}{x^5} \sin(x-u) + \dots \quad (\text{A6})$$

$$= \frac{6}{[kc_s(\eta)\eta]^2} \left[ 1 - \mathcal{O}\left(\frac{1}{x} \frac{\eta_a^4}{\eta^4}\right) \right]. \quad (\text{A7})$$

As expected the transfer function falls off as  $\sim \mathcal{H}^2/(k^2 c_s^2)|_\epsilon$  on small scales with suppressed oscillations. This power-law falloff will only hold on scales where baryon diffusion can be neglected; on ultrasmall scales the spectrum will be exponentially damped. Baryon pressure becomes important at  $k_{\text{pressure}} \sim 1/(c_s(\eta_*)\eta_*)$ , diffusion damping will become important at  $k_{\text{diffusion}} \sim$

$k_{\text{pressure}}(\eta/\eta_{\text{coll}})_{\text{min}}^{1/2}$  where  $\eta_{\text{coll}}$  is the atomic collision time, which is always much smaller than  $\eta$  (see Fig. 1).

At redshifts of 30 to 100 residual Compton coupling actually gives  $c_s$  scaling as  $\eta^{-1.9}$  to  $\eta^{-1.6}$ , and approximating the transition in cooling behavior as sharp may be expected to be a poor approximation on scales such that  $kc_s(\eta_a)\eta_a \gg 1$ . In this limit, the following approximation can be used:

$$\Delta_b(\eta)/\Delta_c(\eta) = \frac{6}{\eta^3} \int_{\eta_*}^{\eta} \frac{\eta'}{k\sqrt{c_s(\eta)c_s(\eta')}} \times \sin\left(\int_{\eta'}^{\eta} kc_s(\eta'')d\eta''\right) d\eta'. \quad (\text{A8})$$

This is derived from the WKB solutions of the homogeneous equation with Green's method. It is an exact solution for all  $k$  when the gas is adiabatically cooling, but only holds for  $kc_s(\eta_*)\eta_* \gg 1$  when Compton heating is still important. It can be shown that this result agrees with Eqs. (A3) and (A5) in the limit  $x \gg 1$  (and for a sharp transition to adiabatic cooling).

## APPENDIX B: GENERAL GAUGE AND NUMERICAL CALCULATION

We perform numerical calculations in the synchronous gauge. For convenience we give the equations in a general gauge here. The multipole equations in the 1 + 3 conventions of Refs. [54,55] are

$$\begin{aligned} \dot{F}_l + \frac{k}{2l+1} [(l+1)F_{l+1} - lF_{l-1}] + \left[ \delta_{2l} \frac{2}{15} k\sigma - \delta_{0l} \dot{h} - \delta_{1l} \frac{1}{3} kA \right] \epsilon \partial_\epsilon \bar{f} \\ = a\bar{\rho}_s \delta(\epsilon/a - E_{2l}) \left[ \delta_{l0} (\Delta_s - A) - \frac{T_\gamma}{T_s - T_\gamma} \left\{ \frac{\delta_{1l}}{3} (\mathbf{v}_\gamma - \mathbf{v}) + \sum_{l''=2}^{\infty} \delta_{ll''} \Theta_{l''} \right\} \right] \\ - \dot{\tau}_c \left[ (\delta_{l0} - 1)F_l - \frac{\delta_{1l}}{3} \mathbf{v} \epsilon \partial_\epsilon \bar{f} + \delta_{l2} \frac{F_2}{10} \right] - \dot{\tau} [F_l + \delta_{l0} (\Delta_{HI} - \Delta_{T_s} - A) \bar{f}] - \delta_{1l} \frac{\mathbf{v}}{3} (\partial_\epsilon [\epsilon \dot{\bar{f}}] + \dot{\tau} \epsilon \partial_\epsilon \bar{f}). \end{aligned} \quad (\text{B1})$$

In the Newtonian gauge the acceleration  $A = -\psi$ , the scale factor perturbation  $h = -\phi$ , and the shear  $\sigma = 0$ . In the synchronous gauge  $A = 0$ ,  $h = h_s/6$ , and the shear  $\sigma = (\dot{h}_s + 6\dot{\eta}_s)/2k$ , where  $h_s$  and  $\eta_s$  are the usual synchronous gauge quantities. Equation (B1) is valid in a general gauge but the individual terms are not gauge invariant. In particular, under a change of velocity field,  $u^a \mapsto u^a + w^a$ , the multipoles transform as

$$F_0 \mapsto F_0 - \frac{w}{k} [\dot{f} + \mathcal{H} \epsilon \partial_\epsilon \bar{f}] \quad (\text{B2})$$

$$F_1 \mapsto F_1 + \frac{1}{3} w \epsilon \partial_\epsilon \bar{f} \quad (\text{B3})$$

$$F_l \mapsto F_l \quad (l > 1). \quad (\text{B4})$$

For completeness, the other variables in Eq. (B1) transform as

$$\dot{h} \mapsto \dot{h} - \frac{1}{k} (\dot{w} \mathcal{H} + w \dot{\mathcal{H}}) + \frac{1}{3} k w, \quad (\text{B5})$$

$$\sigma \mapsto \sigma + w, \quad (\text{B6})$$

$$A \mapsto A + \frac{\dot{w}}{k} + \frac{\mathcal{H} w}{k}, \quad (\text{B7})$$

$$\Delta_s \mapsto \Delta_s - \frac{\dot{\rho}_s}{\bar{\rho}_s} \frac{w}{k}, \quad (\text{B8})$$

$$\mathbf{v} \mapsto \mathbf{v} - w. \quad (\text{B9})$$



With these relations, one can establish the gauge independence of Eq. (B1).

The line-of-sight solution is

$$\begin{aligned}
F_l = e^{-\tau_\epsilon} \int d\eta e^{-\tau_\epsilon + \bar{\tau}} & \left\{ [a\bar{\rho}_s(\Delta_s - A) - a\bar{\tau}_s(\Delta_{HI} - \Delta_{T_s} - A)\bar{f}] \delta(\epsilon/a - E_{21}) + \dot{h}\epsilon\partial_\epsilon \bar{f} - \dot{\tau}_c F_0 \right\} j_l(k\chi) \\
& - \left( \frac{k\sigma}{3} \epsilon \partial_\epsilon \bar{f} + \dot{\tau}_c \frac{F_2}{4} \right) [3j_l''(k\chi) + j_l(k\chi)] - a \left[ (\bar{\rho}_s - \bar{\tau}_s \bar{f}) \partial_\epsilon [\epsilon \delta(\epsilon/a - E_{21})] v \right. \\
& - \bar{\rho}_s \frac{\bar{T}_\gamma}{\bar{T}_s - \bar{T}_\gamma} (v - v_\gamma) \delta(\epsilon/a - E_{21}) \left. \right] j_l'(k\chi) + (kA - \dot{\tau}_c v) \epsilon \partial_\epsilon \bar{f} j_l'(k\chi) \\
& - a\bar{\rho}_s \delta(\epsilon/a - E_{21}) \frac{\bar{T}_\gamma}{\bar{T}_s - \bar{T}_\gamma} \sum_{l'=2}^{\infty} (2l' + 1) \Theta_{l'} i^{l'} P_{l'} \left( -\frac{i}{k} \frac{d}{d\chi\epsilon} \right) j_l(k\chi) \left. \right\} \quad (B10)
\end{aligned}$$

(for  $l > 1$ ), the spin-temperature perturbation is

$$\begin{aligned}
\Delta_{T_s} - \Delta_{T_\gamma} = (R_\gamma - R_g) \delta C_{10} + C_{10} (R_g \Delta_{T_g} - R_\gamma \Delta_{T_\gamma}) \\
+ \frac{1}{2} \tau_\eta A_{10} C_{10} \frac{\bar{T}_g - \bar{T}_\gamma}{T_\star} R_g R_\gamma \left[ \Delta_{HI} - \frac{\dot{h}}{\mathcal{H}} \right. \\
- \frac{kv}{3\mathcal{H}} - A + \Delta_{C_{10}} + 2\Delta_{T_\gamma} (C_{10} R_\gamma - 1) \\
\left. - 2R_\gamma \delta C_{10} + \frac{\bar{T}_\gamma}{\bar{T}_g - \bar{T}_\gamma} (\Delta_{T_g} - \Delta_{T_\gamma}) \right], \quad (B11)
\end{aligned}$$

and the gas temperature perturbations evolve with

$$\begin{aligned}
\dot{\Delta}_{T_g} = -\frac{2}{3} kv - 2\dot{h} - \frac{8a\sigma_T \bar{\rho}_\gamma \bar{x}_e}{3m_e c(1 + f_{\text{He}} + \bar{x}_e)} \left[ \left( 1 - \frac{\bar{T}_\gamma}{\bar{T}_g} \right) \right. \\
\times \left. \left[ 4\Delta_{T_\gamma} - A + \frac{\Delta_{x_e}}{1 + \bar{x}_e/(1 + f_{\text{He}})} \right] \right. \\
\left. + \frac{\bar{T}_\gamma}{\bar{T}_g} (\Delta_{T_g} - \Delta_{T_\gamma}) \right], \quad (B12)
\end{aligned}$$

where we again neglected helium fraction perturbations. Equation (35) in the main text holds in any gauge.

We choose to work in the synchronous gauge, evaluating the line-of-sight solution integrated over a frequency window function. We use the synchronous gauge because this is stable for isocurvature mode evolution, and because conventional calculations invariably use the baryon (or CDM) power spectrum in the synchronous gauge as output by CMBFAST or CAMB. Since both  $v - v_c$  and  $\tau_\eta$  are small on scales where our calculation is applicable (much larger than the linewidth), in the synchronous gauge ( $v_c = 0$ ) terms involving  $\tau_\eta v$  can be dropped to good accuracy.

We define a window function  $W_f(\epsilon)$  so that we observe  $\int d\epsilon W_f(\epsilon) f$ . Then integrating over energies, assuming the window function is much broader than the linewidth, we use the functions

$$\begin{aligned}
G(\eta) & \equiv \int d\epsilon e^{\bar{\tau} - \tau_\epsilon} W_f(\epsilon) a \bar{\rho}_s \delta(\epsilon/a - E_{21}) \\
& = \frac{1 - e^{-\tau_\eta}}{\tau_\eta} a^2 \bar{\rho}_s W_f(\epsilon_\eta) \quad (B13)
\end{aligned}$$

$$\begin{aligned}
G_\tau(\eta) & \equiv \int d\epsilon e^{\bar{\tau} - \tau_\epsilon} W_f(\epsilon) a \bar{\tau}_s \bar{f} \delta(\epsilon/a - E_{21}) \\
& = \left[ 1 - \frac{\tau_\eta e^{-\tau_\eta}}{1 - e^{-\tau_\eta}} \right] G(\eta) \quad (B14)
\end{aligned}$$

$$\begin{aligned}
V(\eta) & \equiv \int d\epsilon e^{\bar{\tau} - \tau_\epsilon} W_f(\epsilon) \epsilon \partial_\epsilon \bar{f} \\
& = -e^{-\tau_\eta} \frac{a^2 \bar{\rho}_s}{\mathcal{H}} W_f(\epsilon_\eta) + \int^\eta d\eta' a(\eta') \frac{\partial}{\partial \eta'} \\
& \times \left( \frac{1 - e^{-\tau_{\eta'}}}{\tau_{\eta'}} \frac{a(\eta') \bar{\rho}_s(\eta')}{\mathcal{H}(\eta')} \right) W_f(\epsilon_{\eta'}), \quad (B15)
\end{aligned}$$

where  $W_f(\epsilon) = -W_f(z)E_{21}/\epsilon^2 = W_f(a)/E_{21}$ . For 21 cm we assume we measure some averaged brightness temperature

$$\bar{T}_b = \int d\nu W_T(\nu) T_b(\nu). \quad (B16)$$

Then

$$\bar{T}_b = \int da W_T(a) \frac{ch_p^3}{2k_B} \epsilon f, \quad (B17)$$

where  $W_T(a)$  is a window over dimensionless frequency, so

$$W_f(\epsilon) = \frac{ch_p^3}{2k_B} a W_T(a). \quad (B18)$$

### APPENDIX C: EVALUATION OF $\mathcal{N}_{\nu 0}$

The contribution from radiative transitions in the 21 cm line to the evolution of the spin temperature is

$$\begin{aligned} \frac{\partial \beta_s}{\partial \tau} &= \beta_* \left(1 + \frac{N_1}{N_0}\right) \left[ (1 + \mathcal{N}_{\nu 0}) A_{10} - 3 \frac{N_0}{N_1} A_{10} \mathcal{N}_{\nu 0} \right] \\ &\approx 4\beta_* A_{10} \left(1 - \frac{\beta_s}{\beta_*} \mathcal{N}_{\nu 0}\right). \end{aligned} \quad (\text{C1})$$

Here, recall  $\mathcal{N}_{\nu 0}$  is the isotropic part (in the gas rest frame) of the photon occupation number integrated over the line profile. The occupation number has contributions from the background and perturbed CMB and the 21-cm line radiation, i.e.

$$\mathcal{N}_{\nu} = \frac{k_B \bar{T}_\gamma}{E} (1 + \Theta) + \frac{h_p^3}{2} (\bar{f} + \delta f), \quad (\text{C2})$$

making the Rayleigh-Jeans' approximation for the CMB. Evaluating

$$\begin{aligned} \mathcal{N}_{\nu 0} &= \frac{1}{4\pi} \int d\tilde{E} d\tilde{\Omega} \mathcal{N}(\tilde{E}, \tilde{\mathbf{e}}) \Phi(\tilde{E} - E_{21}) \\ &= \frac{1}{4\pi} \int dE d\Omega \frac{E}{\bar{E}} \mathcal{N}(E, \mathbf{e}) \Phi(\tilde{E} - E_{21}) \end{aligned} \quad (\text{C3})$$

for the CMB, we find

$$\mathcal{N}_{\nu 0}^{(\text{CMB})} = \frac{\bar{T}_\gamma}{T_*} (1 + \Delta_{T_\gamma}). \quad (\text{C4})$$

The 21 cm part takes more work. First, consider the contribution from  $\delta f$ ; since  $\delta f$  is first order, we only require its monopole in the conformal Newtonian gauge. As we are integrating over the line profile, at any time  $\eta$  we are including only 21-cm radiation that was ‘‘produced’’ at earlier times within a narrow time window  $\Delta\eta \sim \Delta E / (\mathcal{H} E_{21})$  where  $\Delta E$  is the linewidth. We therefore generalize Eq. (18) for  $\epsilon$  very close to  $\epsilon_\eta$  under the assumption that the perturbations have (comoving) wavelength  $\gg \Delta\eta$ . Extracting the monopole, we find

$$\begin{aligned} \frac{h_p^3}{2} \delta f_0(\eta, \mathbf{x}, \epsilon) &\approx \left(\frac{\bar{T}_s - \bar{T}_\gamma}{T_*}\right) \epsilon \left[ \frac{1}{\mathcal{H}} \left(\phi - \frac{1}{3} \nabla \cdot \mathbf{v}\right) \bar{\tau} e^{-\bar{\tau}} \right. \\ &\quad \left. + (\Delta_s + \psi)(1 - e^{-\bar{\tau}}) - (\Delta_{H_I} - \Delta_{T_s} + \psi) \right. \\ &\quad \left. \times [1 - (1 + \bar{\tau})e^{-\bar{\tau}}] \right]. \end{aligned} \quad (\text{C5})$$

The divergence of the gas velocity arises here from the monopole of the redshift-space distortion:

$$\frac{1}{4\pi} \int d\Omega \mathbf{e} \cdot (\mathbf{e} \cdot \nabla \mathbf{v}) = \frac{1}{3} \nabla \cdot \mathbf{v}. \quad (\text{C6})$$

Integrating over the line profile, we obtain the following contribution to  $\mathcal{N}_{\nu 0}$  from 21 cm perturbations:

$$\begin{aligned} \mathcal{N}_{\nu 0}^{(\delta f)} &= \left(\frac{\bar{T}_s - \bar{T}_\gamma}{T_*}\right) \left[ (\Delta_s + \psi) \left(1 - \frac{1 - e^{-\tau_\eta}}{\tau_\eta}\right) \right. \\ &\quad \left. - (\Delta_{H_I} - \Delta_{T_s} + \psi) \left(1 + e^{-\tau_\eta} - 2 \frac{1 - e^{-\tau_\eta}}{\tau_\eta}\right) \right. \\ &\quad \left. + \frac{1}{\mathcal{H}} \left(\phi - \frac{1}{3} \nabla \cdot \mathbf{v}\right) \left(\frac{1 - e^{-\tau_\eta}}{\tau_\eta} - e^{-\tau_\eta}\right) \right]. \end{aligned} \quad (\text{C7})$$

We also need the contribution from  $\bar{f}$ . Correct to linear order in  $\mathbf{v}$ , this is simply

$$\mathcal{N}_{\nu 0}^{(\bar{f})} = \left(\frac{\bar{T}_s - \bar{T}_\gamma}{T_*}\right) \left(1 - \frac{1 - e^{-\tau_\eta}}{\tau_\eta}\right); \quad (\text{C8})$$

nonlinear corrections in  $\mathbf{v}$  may be important if  $E_{21} |\mathbf{v}| \gtrsim \Delta E$ . Combining all results, and expanding to first order in  $\tau_\eta$ , we obtain our desired result:

$$\begin{aligned} \mathcal{N}_{\nu 0} &\approx \frac{\bar{T}_\gamma}{T_*} (1 + \Delta_{T_\gamma}) + \frac{\tau_\eta}{2} \left(\frac{\bar{T}_s - \bar{T}_\gamma}{T_*}\right) \left[ 1 + \Delta_s + \psi \right. \\ &\quad \left. + \frac{1}{\mathcal{H}} \left(\phi - \frac{1}{3} \nabla \cdot \mathbf{v}\right) \right]. \end{aligned} \quad (\text{C9})$$

In this approximation, the perturbed Rayleigh-Jeans' brightness temperature,  $T_* \mathcal{N}_{\nu 0}$ , that we use in the main text is

$$\begin{aligned} T_\gamma + T_{b0} &= \bar{T}_\gamma (1 + \Delta_{T_\gamma}) + \frac{\tau_\eta}{2} (\bar{T}_s - \bar{T}_\gamma) \\ &\quad \times \left[ 1 + \Delta_s + \psi + \frac{1}{\mathcal{H}} \left(\phi - \frac{1}{3} \nabla \cdot \mathbf{v}\right) \right]. \end{aligned} \quad (\text{C10})$$

As we might have anticipated, this can be expressed in terms of the (perturbed) optical depth  $\hat{\tau}_\eta$  of Eq. (30), and the monopole of the CMB temperature  $T_\gamma$  as  $T_{b0} = \hat{\tau}_\eta (T_s - T_\gamma) / 2$ .

## APPENDIX D: IONIZATION FRACTION PERTURBATIONS

For our approximate analysis of ionization fraction perturbations, we start the perturbation evolution after helium has recombined, so we take  $n_{HI} = (1 - x_e) n_H$  and  $n_e = x_e n_H$  where  $n_H$  is the total number density of ionized and unionized hydrogen. We then use the effective equation of RECFAST [22]

$$\dot{x}_e = -a C_r (x_e^2 n_H \alpha - \beta (1 - x_e) e^{-E_{H2s}/k_B T_s}), \quad (\text{D1})$$

where  $E_{H2s}$  is the energy of the transition from the ground to the  $2s$  state and

$$C_r \equiv \frac{1 + \mathcal{K} \Lambda n_H (1 - x_e)}{1 + \mathcal{K} (\Lambda + \beta) n_H (1 - x_e)}. \quad (\text{D2})$$

The recombination and photoionization coefficients are related by

$$\beta = \alpha \left( \frac{m_e k_B T_g}{2\pi \hbar^2} \right)^{3/2} e^{-E_{2s}/k_B T_g}, \quad (\text{D3})$$

where  $E_{2s}$  is the ionization energy from the  $2s$  state, and  $\alpha$  is also a function of the temperature fit by

$$\alpha = F \frac{a_\alpha (T_g/10^4 \text{ K})^b}{1 + c(T_g/10^4 \text{ K})^d} \text{ m}^3 \text{ s}^{-1}. \quad (\text{D4})$$

Here  $F$  is a fudge factor taken to be 1.14 and  $a_\alpha = 4.309 \times 10^{-19}$ ,  $b = -0.6166$ ,  $c = 0.6703$ ,  $d = 0.5300$ . The constant two photon  $2s-1s$  decay rate is  $\Lambda = 8.22458 \text{ s}^{-1}$ . Dependence on the expansion rate enters through the cosmological redshifting term  $\mathcal{K}$ , given in the background by  $\mathcal{K} = a\lambda_{\text{H}2p}^3/(8\pi\mathcal{H})$ .

A perturbed version of Eq. (D1) may be inappropriate due to the effect of perturbation velocities on the escape probabilities that went into deriving the result. However, the detailed perturbation evolution during recombination does not affect the 21 cm absorption signal as long as the residual perturbations after recombination are correct, at

which point recombination is limited solely by the low rate of electron capture to an excited state. A full analysis is beyond the scope of this paper, so we proceed from the perturbed version of Eq. (D1) and argue this is sufficient:

$$\begin{aligned} \dot{\Delta}_{x_e} = & \frac{\dot{x}_e}{x_e} (\Delta_{C_r} + \Delta_\alpha - \Delta_{x_e} - A) \\ & - aC_r \left\{ (2\Delta_{x_e} + \Delta_{\text{H}}) \alpha x_e n_{\text{H}} \right. \\ & \left. + \left\{ \Delta_{x_e} - \left( \frac{3}{2} + \frac{E_{2s}}{k_B T_g} \right) \left( \frac{1}{x_e} - 1 \right) \Delta_{T_g} \right\} \beta e^{-E_{\text{H}2s}/k_B T_g} \right\}. \end{aligned} \quad (\text{D5})$$

We generalize  $\mathcal{K}$  to a perturbed universe as  $\mathcal{K} = 3\lambda_{\text{H}2p}^3/(8\pi\nabla_a u_g^a)$  to account for the local baryon expansion rate; this should be correct on scales sufficiently large compared to the mean Lyman- $\alpha$  photon interaction length (which is very short). The perturbed terms are then

$$\Delta_{C_r} = - \frac{\beta \mathcal{K} n_{\text{H}} \{ [\Delta_{\text{H}} + \Delta_{\mathcal{K}} + \Delta_\beta (1 + \mathcal{K} \Lambda n_{\text{H}} (1 - x_e))] (1 - x_e) - x_e \Delta_{x_e} \}}{(1 + \mathcal{K} \Lambda n_{\text{H}} (1 - x_e)) (1 + \mathcal{K} (\beta + \Lambda) n_{\text{H}} (1 - x_e))} \quad (\text{D6})$$

$$\Delta_\beta = \Delta_\alpha + \left( \frac{3}{2} + \frac{E_{2s}}{k_B T_g} \right) \Delta_{T_g} \quad (\text{D7})$$

$$\Delta_\alpha = \frac{b + c(T_g/10^4 \text{ K})^d (b - d)}{1 + c(T_g/10^4 \text{ K})^d} \Delta_{T_g} \quad (\text{D8})$$

$$\Delta_{\mathcal{K}} = - \frac{\dot{h}}{\mathcal{H}} - \frac{kv}{3\mathcal{H}} - A. \quad (\text{D9})$$

In the synchronous gauge the dominant term on large scales is initially due to fluctuations in the expansion rate,  $\Delta_{\mathcal{K}} \sim \dot{\Delta}_b/3\mathcal{H}$ :  $\Delta_{x_e}$  is the same sign as  $\Delta_c$  because overdensities expand less fast and hence have a higher ionization fraction than the average ( $\Delta_{\mathcal{K}}$  appears to have been ignored in e.g. Refs. [56,57]). At later times when  $x_e \ll 1$  the main effect is from perturbations in the hydrogen density and temperature; this leads to  $\Delta_{x_e}$  being the opposite sign to  $\Delta_c$  at late times because overdensities recombine more efficiently. Note that at late times some terms in Eq. (D5) are invalid because  $\Delta_{T_g} E_i/k_B T_g$  becomes of order unity, however the error is harmless because the entire term is exponentially suppressed: at late times the evolution is given approximately by

$$\dot{x}_e \approx -a\alpha x_e^2 n_{\text{H}} \quad (\text{D10})$$

$$\dot{\Delta}_{x_e} \approx -a\alpha x_e n_{\text{H}} (\Delta_\alpha + \Delta_{x_e} + \Delta_{\text{H}}). \quad (\text{D11})$$

It is not necessary to model the early evolution correctly to get approximately the correct late-time answer. Indeed the

late-time evolution neglecting velocity effects should be quite accurate as recombination is limited by the low electron capture probability. However, the overall ionization fraction evolution is limited by the precision of the RECFAST model, in which a single fudge factor accounts for deviations of an effective three level atom model from the full result.

Using the equations given here, the effect on the 21 cm power spectrum of neglecting  $\Delta_{x_e}$  is  $\mathcal{O}(2\%)$  at  $z \sim 50$ , almost entirely due to the indirect effect on the evolution of the temperature perturbation. Note that, at the Jeans' scale, ionization fraction perturbations also have a linear effect on the baryon density evolution due to the modified evolution of the gas temperature perturbation (and hence the baryon pressure perturbation).

## APPENDIX E: SPHERICAL BESSEL FUNCTION INTEGRALS AND APPROXIMATIONS

Integrals of products of spherical Bessel functions can be done analytically using the result [58]

$$\begin{aligned} & \int_0^\infty dr j_l(r) j_{l'}(r) r^{-n} \\ & = \frac{\pi \Gamma(n+1) \Gamma(\frac{l+l'+1-n}{2})}{2^{n+2} \Gamma(\frac{l-l'+2+n}{2}) \Gamma(\frac{l+l'+3+n}{2}) \Gamma(\frac{l-l'+2+n}{2})}. \end{aligned} \quad (\text{E1})$$

In particular, using this result in combination with the spherical Bessel equation, we have

$$l(l+1) \int_{-\infty}^{\infty} d \ln r [j_l(r)]^2 = \frac{1}{2} \quad (\text{E2})$$

$$l(l+1) \int_{-\infty}^{\infty} d \ln r j_l(r) j_l''(r) = -\frac{1}{6} \quad (\text{E3})$$

$$l(l+1) \int_{-\infty}^{\infty} d \ln r [j_l''(r)]^2 = \frac{1}{10} + \frac{4}{15(l-2)(l+3)} \approx \frac{1}{10}, \quad (\text{E4})$$

where the approximation holds for high  $l$  of most interest in this paper.

At high  $l$  the Bessel functions oscillate very rapidly compared to the scale of variation in the power spectra. Direct numerical integration becomes slow, but quite accurate results can be obtained by averaging over the oscillations. Defining  $\nu \equiv l + 1/2$ , for  $r^2/\nu^2 \gtrsim 1 + \nu^{-2/3}$  we can use the approximation [58]

$$j_l(r) \approx \frac{\sin(\sqrt{r^2 - \nu^2} - \arccos(\nu/r)/\nu + \pi/4)}{r(1 - \nu^2/r^2)^{1/4}}. \quad (\text{E5})$$

Neglecting oscillatory parts that closely average to zero, we then have for  $l \gg 1$

$$\langle [j_l(r)]^2 \rangle \sim \frac{1}{2r\sqrt{r^2 - \nu^2}} \quad (\text{E6})$$

$$\langle [j_l''(r)]^2 \rangle \sim \frac{(r^2 - \nu^2)^{3/2}}{2r^5} \quad (\text{E7})$$

$$\langle j_l''(r) j_l(r) \rangle \sim -\frac{\sqrt{r^2 - \nu^2}}{2r^3}. \quad (\text{E8})$$

## APPENDIX F: NONLINEAR CDM POWER SPECTRA

At a given redshift, the two leading corrections to the power spectrum are given in terms of the linear-theory matter power spectrum at that redshift,  $\mathcal{P}(k) \equiv k^3 P(k)/(2\pi^2)$ , by [35,36,38,59]

$$\begin{aligned} \mathcal{P}_{13}(k) &= \int_0^{\infty} dr I_{13}(k, r) \\ &\equiv \frac{\mathcal{P}(k)}{504} \int_{-\infty}^{\infty} d \ln r \mathcal{P}(kr) \left[ \frac{12}{r^4} - \frac{158}{r^2} + 100 - 42r^2 \right. \\ &\quad \left. + \frac{3}{r^5} (r^2 - 1)^3 (7r^2 + 2) \ln \left| \frac{1+r}{1-r} \right| \right] \end{aligned} \quad (\text{F1})$$

and

$$\begin{aligned} \mathcal{P}_{22}(k) &= \int_0^{\infty} dr \int_{-1}^1 dx I_{22}(k, r, x) \\ &\equiv \frac{1}{196} \int_{-\infty}^{\infty} d \ln r \mathcal{P}(kr) \\ &\quad \times \int_{-1}^1 dx \mathcal{P}(k[1+r^2-2rx]^{1/2}) \\ &\quad \times \frac{(3r+7x-10rx^2)^2}{r^2(1+r^2-2rx)^{7/2}}. \end{aligned} \quad (\text{F2})$$

For the small scales of interest to us here, the dominant contribution comes from  $q \lesssim k$ , with significant mode coupling to all scales where the spectrum is growing logarithmically. This can become numerically difficult because for  $r \ll 1$  the two terms  $\mathcal{P}_{22}$  and  $\mathcal{P}_{13}$  become large but almost cancel. For  $r < r_s$  we therefore use an approximate series expansion, switching to the full result at  $r > r_s$ . The expression for the correction to the matter power spectrum can then be written

$$\begin{aligned} \mathcal{P}_{13}(k) + \mathcal{P}_{22}(k) &\approx \left[ \frac{8126}{2205} - \frac{22}{21} \frac{d \ln \mathcal{P}}{d \ln k} + \frac{1}{10} \left\{ \left( \frac{d \ln \mathcal{P}}{d \ln k} \right)^2 + \frac{d^2 \ln \mathcal{P}}{d (\ln k)^2} \right\} \right] \mathcal{P}(k) \int_{-\infty}^{\ln r_s} d \ln r \mathcal{P}(kr) + \int_{r_s}^{\infty} dr I_{13}(k, r) \\ &\quad + \left[ 2 \int_{r_s}^{\epsilon} dr \int_{-1}^1 dx + \int_{\epsilon}^{1-\epsilon} dr \int_{-1}^1 dx + \int_{1-\epsilon}^{1+\epsilon} dr \int_{-1}^{(1+r^2-\epsilon^2)/2r} dx + \int_{1+\epsilon}^{\infty} dr \int_{-1}^1 dx \right] I_{22}(k, r, x), \end{aligned} \quad (\text{F3})$$

where  $r_s < \epsilon \leq 1/2$  (numerically it is better to choose  $\epsilon \sim 1/2$ ). For a scale-invariant primordial spectrum the small-scale power spectrum is  $\mathcal{P}(kr) \sim \mathcal{P}(k)[1 - \ln(r)/\ln(r_0)]^2$ , where  $r_0$  corresponds to the much larger scale  $k_0$  where logarithmic growth starts. The main nonlinear contribution to the power spectrum can then be approximated from the first term in Eq. (F3) as  $\sim -\ln(r_0)[\mathcal{P}(k)]^2 \sim \ln(k/k_0) \times [\mathcal{P}(k)]^2$ . On the Jeans' scale at  $z = 50$ , this implies a fractional second-order contribution to the power spectrum of  $\sim \mathcal{O}(10)\mathcal{P}(k)$ : on small scales nonlinear effects are more important than one might naively think [37]. See Fig. 10 for typical numerical results.

The 21 cm angular-power spectrum on small scales is also sensitive to redshift distortions, for which we need to estimate the second-order velocity power spectrum and the cross correlation with the density. The results are similar to those for the density with

$$\begin{aligned} \mathcal{P}_{13}^{vv}(k) &= \frac{\mathcal{P}(k)}{168} \int_{-\infty}^{\infty} d \ln r \mathcal{P}(kr) \left[ \frac{12}{r^4} - \frac{82}{r^2} + 4 - 6r^2 \right. \\ &\quad \left. + \frac{3}{r^5} (r^2 - 1)^3 (r^2 + 2) \ln \left| \frac{1+r}{1-r} \right| \right], \end{aligned} \quad (\text{F4})$$

and

$$\begin{aligned} \mathcal{P}_{22}^{vv}(k) &= \frac{1}{196} \int_{-\infty}^{\infty} d \ln r \mathcal{P}(kr) \\ &\times \int_{-1}^1 dx \mathcal{P}(k[1+r^2-2rx]^{1/2}) \\ &\times \frac{(r-7x+6rx^2)^2}{r^2(1+r^2-2rx)^{7/2}}, \end{aligned} \quad (\text{F5})$$

where  $\mathcal{P}^{vv}$  is the power spectrum of  $kv/\mathcal{H}$ . The series result for use at high  $l$  is

$$\begin{aligned} \mathcal{P}_{13}^{vv}(k) + \mathcal{P}_{22}^{vv}(k) &\approx \left[ \frac{558}{245} - \frac{94}{105} \frac{d \ln \mathcal{P}}{d \ln k} + \frac{1}{10} \left\{ \left( \frac{d \ln \mathcal{P}}{d \ln k} \right)^2 \right. \right. \\ &\left. \left. + \frac{d^2 \ln \mathcal{P}}{d(\ln k)^2} \right\} \right] \mathcal{P}(k) \int_{-\infty}^{\ln r_s} d \ln r \mathcal{P}(kr). \end{aligned} \quad (\text{F6})$$

Similarly the cross-correlation power spectrum is given by

$$\begin{aligned} \mathcal{P}_{13}^{v\delta}(k) &= -\frac{\mathcal{P}(k)}{504} \int_{-\infty}^{\infty} d \ln r \mathcal{P}(kr) \left[ \frac{24}{r^4} - \frac{202}{r^2} + 56 \right. \\ &\left. - 30r^2 + \frac{3}{r^5}(r^2-1)^3(5r^2+4) \ln \left| \frac{1+r}{1-r} \right| \right] \end{aligned} \quad (\text{F7})$$

and

$$\begin{aligned} \mathcal{P}_{22}^{v\delta}(k) &= -\frac{1}{196} \int_{-\infty}^{\infty} d \ln r \mathcal{P}(kr) \\ &\times \int_{-1}^1 dx \mathcal{P}(k[1+r^2-2rx]^{1/2}) \\ &\times \frac{(r-7x+6rx^2)(-3r-7x+10rx^2)}{r^2(1+r^2-2rx)^{7/2}}, \end{aligned} \quad (\text{F8})$$

with the series result

$$\begin{aligned} \mathcal{P}_{13}^{v\delta}(k) + \mathcal{P}_{22}^{v\delta}(k) &\approx -\left[ \frac{6382}{2205} - \frac{34}{35} \frac{d \ln \mathcal{P}}{d \ln k} \right. \\ &\left. + \frac{1}{10} \left\{ \left( \frac{d \ln \mathcal{P}}{d \ln k} \right)^2 + \frac{d^2 \ln \mathcal{P}}{d(\ln k)^2} \right\} \right] \\ &\times \mathcal{P}(k) \int_{-\infty}^{\ln r_s} d \ln r \mathcal{P}(kr). \end{aligned} \quad (\text{F9})$$

- 
- [1] D. Scott and M.J. Rees, *Mon. Not. R. Astron. Soc.* **247**, 510 (1990).  
[2] A. Loeb and M. Zaldarriaga, *Phys. Rev. Lett.* **92**, 211301 (2004).  
[3] S. Furlanetto, S.P. Oh, and F. Briggs, *Phys. Rep.* **433**, 181 (2006).  
[4] M. Kleban, K. Sigurdson, and I. Swanson, *J. Cosmol. Astropart. Phys.* **08** (2007) 009.  
[5] C.L. Carilli, J.N. Hewitt, and A. Loeb, *arXiv:astro-ph/0702070*.  
[6] R. Barkana and A. Loeb, *Astrophys. J.* **624**, L65 (2005).  
[7] M. Zaldarriaga, S.R. Furlanetto, and L. Hernquist, *Astrophys. J.* **608**, 622 (2004).  
[8] S. Bharadwaj and S.S. Ali, *Mon. Not. R. Astron. Soc.* **352**, 142 (2004).  
[9] S. Naoz and R. Barkana, *Mon. Not. R. Astron. Soc.* **362**, 1047 (2005).  
[10] R. Barkana and A. Loeb, *Mon. Not. R. Astron. Soc. Lett.* **363**, L36 (2005).  
[11] C. Gordon and A. Lewis, *Phys. Rev. D* **67**, 123513 (2003).  
[12] Y.A. Shchekinov and E.O. Vasiliev, *Mon. Not. R. Astron. Soc.* **379**, 1003 (2007).  
[13] S. Furlanetto, S.P. Oh, and E. Pierpaoli, *Phys. Rev. D* **74**, 103502 (2006).  
[14] A. Cooray, *Phys. Rev. Lett.* **97**, 261301 (2006).  
[15] A. Pillepich, C. Porciani, and S. Matarrese, *Astrophys. J.* **662**, 1 (2007).  
[16] M. Valdes, A. Ferrara, M. Mapelli, and E. Ripamonti, *Mon. Not. R. Astron. Soc.* **377**, 245 (2007).  
[17] R. Khatri and B.D. Wandelt, *Phys. Rev. Lett.* **98**, 111301 (2007).  
[18] A. Challinor and A. Lewis (unpublished).  
[19] C.M. Hirata and K. Sigurdson, *Mon. Not. R. Astron. Soc.* **375**, 1241 (2007).  
[20] J.P. Wild, *Astrophys. J.* **115**, 206 (1952).  
[21] S. Furlanetto and M. Furlanetto, *Mon. Not. R. Astron. Soc.* **379**, 130 (2007).  
[22] S. Seager, D.D. Sasselov, and D. Scott, *Astrophys. J. Suppl. Ser.* **128**, 407 (2000).  
[23] R. Weymann, *Phys. Fluids* **8**, 2112 (1965).  
[24] A. Loeb and M. Zaldarriaga, *Phys. Rev. D* **71**, 103520 (2005).  
[25] C.-P. Ma and E. Bertschinger, *Astrophys. J.* **455**, 7 (1995).  
[26] U. Seljak and M. Zaldarriaga, *Astrophys. J.* **469**, 437 (1996).  
[27] W. Hu, U. Seljak, M.J. White, and M. Zaldarriaga, *Phys. Rev. D* **57**, 3290 (1998).  
[28] A. Lewis, A. Challinor, and A. Lasenby, *Astrophys. J.* **538**, 473 (2000).  
[29] B.J. Rickett, *Annu. Rev. Astron. Astrophys.* **28**, 561 (1990).  
[30] M.A. Alvarez, E. Komatsu, O. Dore, and P.R. Shapiro, *Astrophys. J.* **647**, 840 (2006).  
[31] K.K. Datta, T.R. Choudhury, and S. Bharadwaj, *Mon. Not. R. Astron. Soc.* **378**, 119 (2007).  
[32] D. Babich and A. Loeb, *Astrophys. J.* **635**, 1 (2005).  
[33] W. Hu and M. White, *Phys. Rev. D* **56**, 596 (1997).  
[34] A. Challinor, *Phys. Rev. D* **62**, 043004 (2000).



- [35] E. T. Vishniac, *Mon. Not. R. Astron. Soc.* **203**, 345 (1983).
- [36] N. Makino, M. Sasaki, and Y. Suto, *Phys. Rev. D* **46**, 585 (1992).
- [37] B. Jain and E. Bertschinger, *Astrophys. J.* **431**, 495 (1994).
- [38] R. Scoccimarro, *Phys. Rev. D* **70**, 083007 (2004).
- [39] P. McDonald, *Phys. Rev. D* **75**, 043514 (2007).
- [40] K. S. Mandel and M. Zaldarriaga, *Astrophys. J.* **647**, 719 (2006).
- [41] U. Seljak, *Astrophys. J.* **463**, 1 (1996).
- [42] A. Challinor and A. Lewis, *Phys. Rev. D* **71**, 103010 (2005).
- [43] A. Lewis and A. Challinor, *Phys. Rep.* **429**, 1 (2006).
- [44] O. Zahn and M. Zaldarriaga, *Astrophys. J.* **653**, 922 (2006).
- [45] R. B. Metcalf and S. D. M. White, arXiv:astro-ph/0611862.
- [46] S. Hilbert, R. B. Metcalf, and S. D. M. White, arXiv:0706.0849.
- [47] A. F. Heavens, S. Matarrese, and L. Verde, *Mon. Not. R. Astron. Soc.* **301**, 797 (1998).
- [48] J. B. Peterson, K. Bandura, and U. L. Pen, arXiv:astro-ph/0606104.
- [49] E. R. Switzer and C. M. Hirata, arXiv:astro-ph/0702145.
- [50] J. A. Rubino-Martin, J. Chluba, and R. A. Sunyaev, *Mon. Not. R. Astron. Soc.* **371**, 1939 (2006).
- [51] <http://camb.info/sources>
- [52] A. Nusser, *Mon. Not. R. Astron. Soc.* **317**, 902 (2000).
- [53] M. Abramowitz and I. A. Stegun, *Handbook of Mathematical Functions* (Dover, New York, 1972), ISBN 0486612724.
- [54] A. Challinor and A. Lasenby, *Astrophys. J.* **513**, 1 (1999).
- [55] A. Lewis and A. Challinor, *Phys. Rev. D* **66**, 023531 (2002).
- [56] G.-C. Liu, K. Yamamoto, N. Sugiyama, and H. Nishioka, *Astrophys. J.* **547**, 1 (2001).
- [57] S. Singh and C.-P. Ma, *Astrophys. J.* **569**, 1 (2002).
- [58] I. S. Gradshteyn and I. M. Ryzhik, *Table of Integrals, Series and Products* (Academic Press, San Diego, 2000), 6th ed., ISBN 0123736374.
- [59] Y. Suto and M. Sasaki, *Phys. Rev. Lett.* **66**, 264 (1991).